Nearly Normal Galaxies

- Elliptical Galaxies & Bulges
- Dwarf Elliptical Galaxies
- Spiral Galaxies

Nearly Normal Galaxies 1: Elliptical Galaxies & Bulges

Review of Properties Discussed

- Elliptical Galaxies have elliptical shapes with no structure
- Old stellar populations
- Very little gas & dust
- M_B ~ -15 to -26
- M / L ~ 1 – (10) ← correlated with luminosity (weakly)

Things Hinted at

- Giant elliptical galaxies do not rotate

  → they are elliptical because random motions are important

- Elliptical galaxies formed by dissipationless collapse

  → stars formed before gas has time to dissipate much & fall into rotationally support disk (i.e., like spirals)

  → stars basically stay at the radius they are formed at (i.e., stars do not “dissipate”)

- Difference between elliptical galaxies & bulges

  → Ellipticals contain no disk component

  → Bulges are at the centers of disks

General Profiles of Elliptical Galaxies

The projected brightness profiles of elliptical galaxies are well fitted by,

$$\log\left(\frac{I}{I_e}\right) = -3.3307217\left[\left(\frac{r}{r_e}\right)^{1/4} - 1\right],$$

where -3.3307217 is chosen such that r_e is the (effective) radius in which half of the total light is contained.

In terms of surface brightness, μ (mag arcsec^{-2} = -2.5 log I),

$$\mu = \mu_e - 8.325 + 8.325\left(\frac{r}{r_e}\right)^{1/4}.$$

This profile is commonly referred to as the $R^{0.25}$ Law. Note that the central surface brightness is μ_e – 8.325.

Luminosity Calculation

- The total luminosity in a circularly symmetry galaxy is,

$$2\int_0^{r_e} I(R)2\pi R dR = \int_0^{\infty} I(R)2\pi R dR = 7.22\pi r_e^2 I_e.$$

Note that the first integral follows from the fact that half of the light of the galaxy is contained within r_e.

Deviations from $R^{0.25}$ Law are sometimes seen at large radii

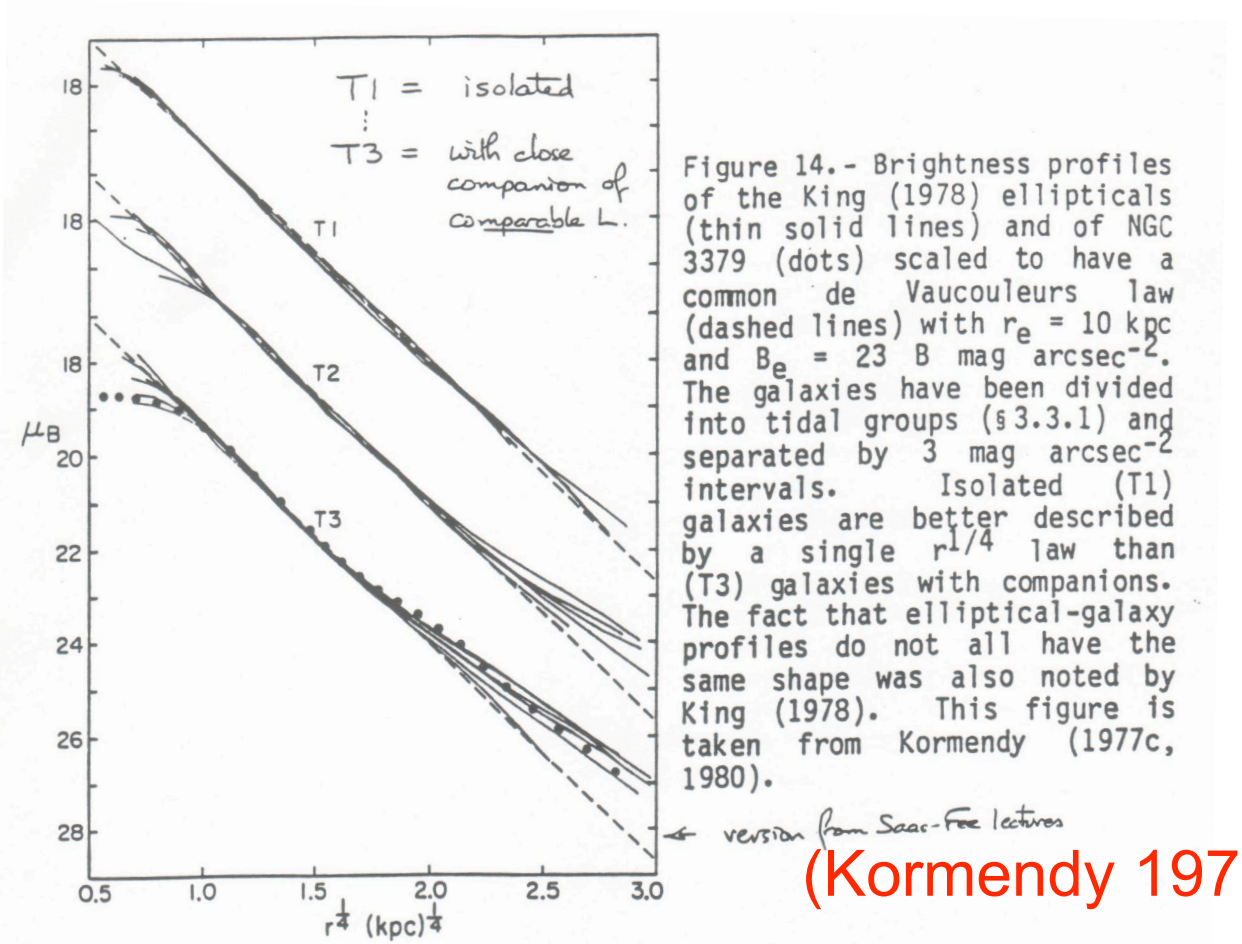

Figure 14.- Brightness profiles of the King (1978) ellipticals (thin solid lines) and of NGC 3379 (dots) scaled to have a common de Vaucouleurs law (dashed lines) with r_e = 10 kpc and B_e = 23 B mag arcsec^{-2}. The galaxies have been divided into tidal groups (§3.3.1) and separated by 3 mag arcsec^{-2} intervals. Isolated (T1) galaxies are better described by a single $r^{1/4}$ law than (T3) galaxies with companions. The fact that elliptical-galaxy profiles do not all have the same shape was also noted by King (1978). This figure is taken from Kormendy (1977c, 1980).

← version from Saas-Fee lectures

(Kormendy 1977, ApJ, 218, 333)

These deviations may be Environmental: correlations are seen between the outer profiles of ellipticals & the presence of companions.

$R^{0.25}$ Deviations may be Luminosity Dependent

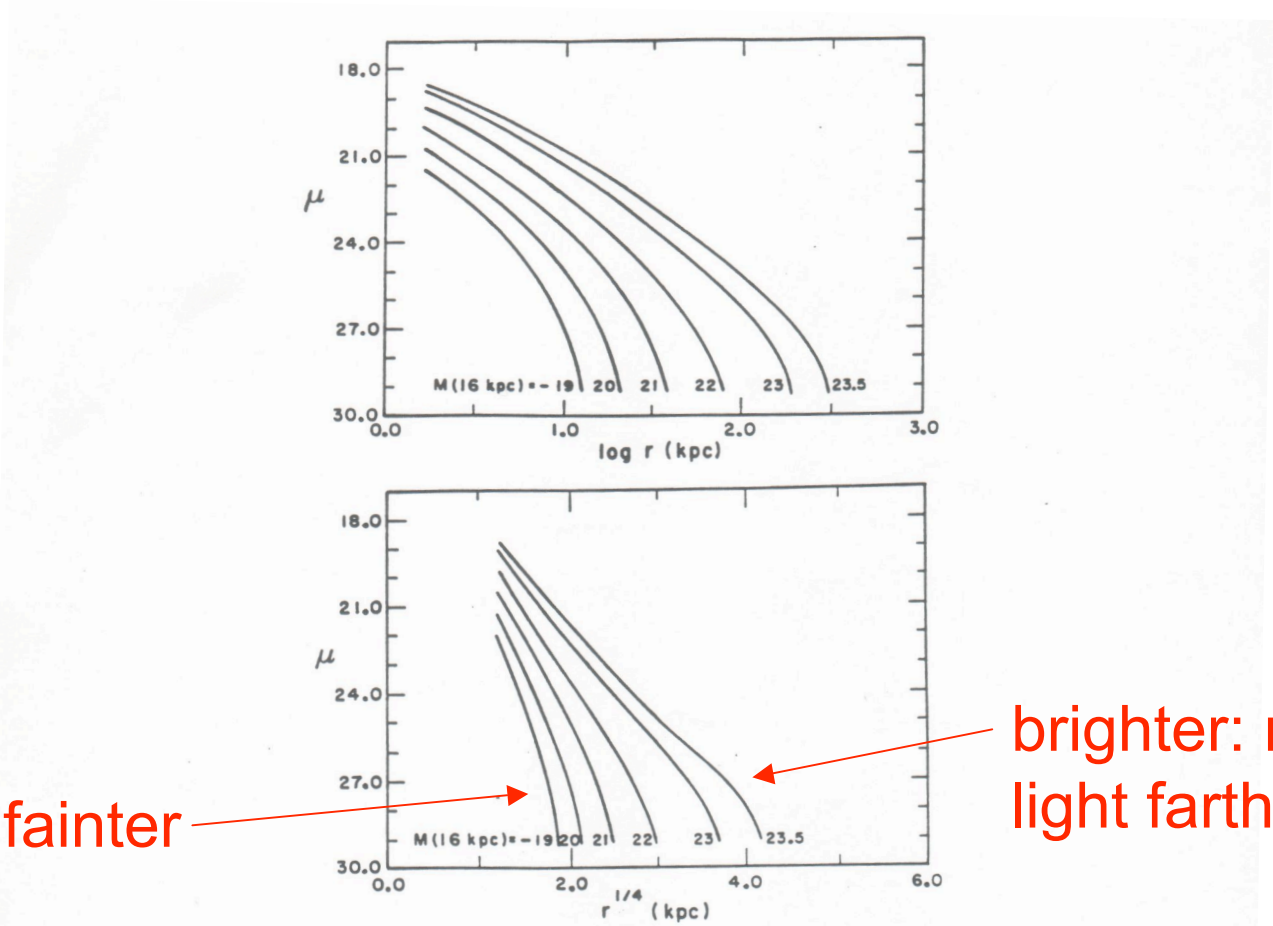

FIG. 14.—Generalized profiles constructed from the linear isophotal radius relations and scaled by the relationship from the upper panel in Fig. 7. Profiles are plotted in both log r and $r^{1/4}$ for comparison with the data in Figs. 1 and 2. Corresponding $M_{16\ \mathrm{kpc}}$ magnitudes are indicated.

fainter

brighter: much more light farther out

(Schombert et al. 1986, ApJS, 60, 603)

- Brighter ellipticals tend to have excess light at large radii, whereas fainter galaxies had too little light at large radii

A Note: cD Galaxies

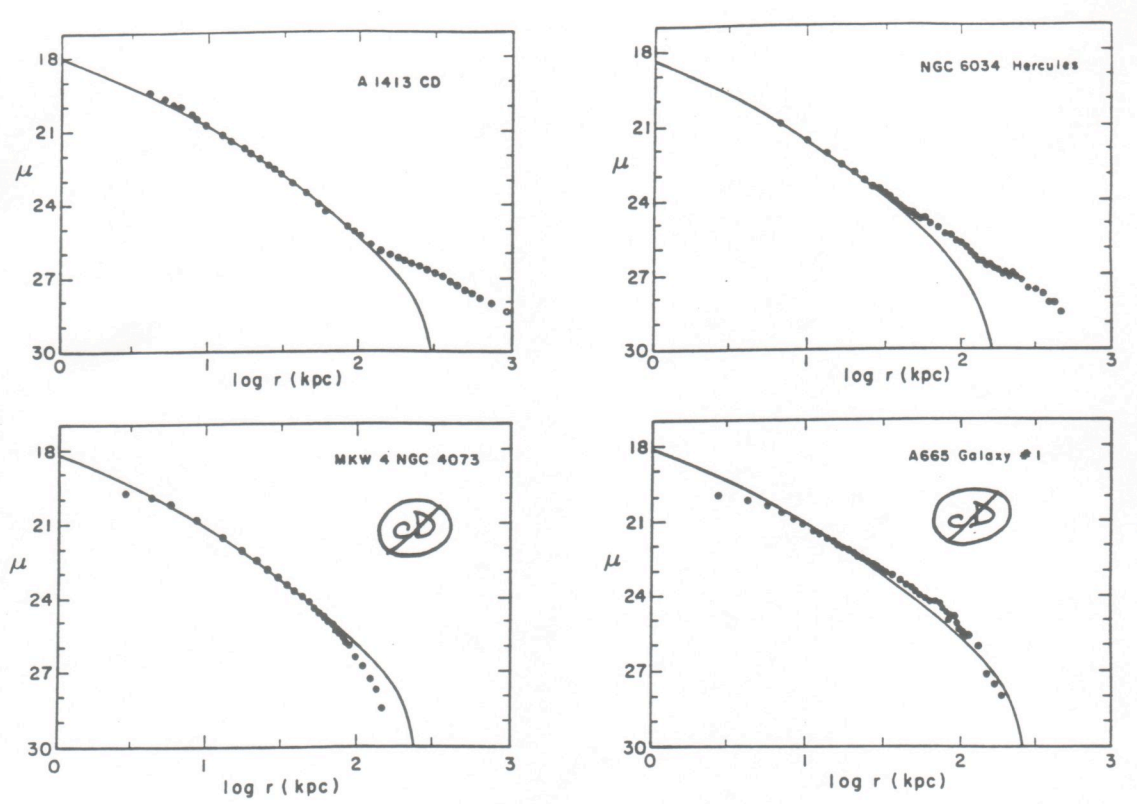

FIG. 17.—Data for A1413, MKW 4, NGC 6034, and A665 Galaxy No. 1 plotted with the best-fit generalized profiles shown as solid lines

- cD galaxies, which are at the centers of clusters, have excess light that appears to be part of the cluster
- The velocity dispersion, σ, of the cD galaxies rises at large radii, and seems to be consistent with the σ of the galaxies in the inner cluster.

The Fundamental Parameter Plane

- Can a fundamental relationship between the measured parameters of elliptical galaxies & bulges be found?

Start with the Virial Theorem,

$$\frac{GM}{\overline{R}} = k_E \frac{\overline{V^2}}{2},$$

where M is the total mass, $GM/\overline{R}$ is the potential energy with mean $\overline{R}$, $\overline{v^2}/2$ is the mean kinetic energy per unit mass, & k_E is the virialization constant.

Let,

$$r_e = k_R \overline{R},$$

where r_e is the scale radius & k_R depends on the density structure. Then

$$L = k_L I_e r_e^2,$$

where I_e is the scale surface brightness, k_L is the constant, & L is the luminosity, and

$$\sigma^2 = k_V \overline{V^2},$$

where σ is the velocity scale.
Substituting these quantities into the Virial Theorem,

$$\frac{GMk_R}{r_e} = \frac{k_E \sigma^2}{2k_V},$$

Two Fundamental Plane Relations

- *R*e – σ – I_e Relation:

$$r_e = \frac{k_E}{2Gk_Rk_Lk_V}\sigma^2 I_e^{-1}\left(\frac{M}{L}\right)^{-1}.$$

- *L* – σ – I_e Relation:

$$L = \frac{k_E^2}{4G^2k_R^2k_Lk_V^2}\sigma^4 I_e^{-1}\left(\frac{M}{L}\right)^{-2}.$$

- If all galaxies have the same structure, then the *k* terms are constant. Thus,

$$r_e = \text{constant} \cdot \sigma^2 I_e^{-1} \left(\frac{M}{L}\right)^{-1};$$

$$L = \text{constant} \cdot \sigma^4 I_e^{-1} \left(\frac{M}{L}\right)^{-2}.$$

- If $M/L \sim L^n I^m$, then the expressions reduce to ,

$$r_e = \text{constant} \cdot \sigma^2 I_e^{-1} \left(L^n I^m\right)^{-1} = \text{constant} \cdot \sigma^2 I_e^{-1} \left(I^{n+m} r_e^{2n}\right)^{-1}$$

$$L = \text{constant} \cdot \sigma^4 I_e^{-1} \left(L^n I^m\right)^{-2}$$

I.e., $r_e = f(\sigma, I_e)$ or $L = f(\sigma, I_e)$

- Note that the second equation looks similar to the Faber-Jackson Relation (1976, ApJ, 204, 668),

$$L \propto \sigma^4$$

FP Relations : Comparison with Real Data

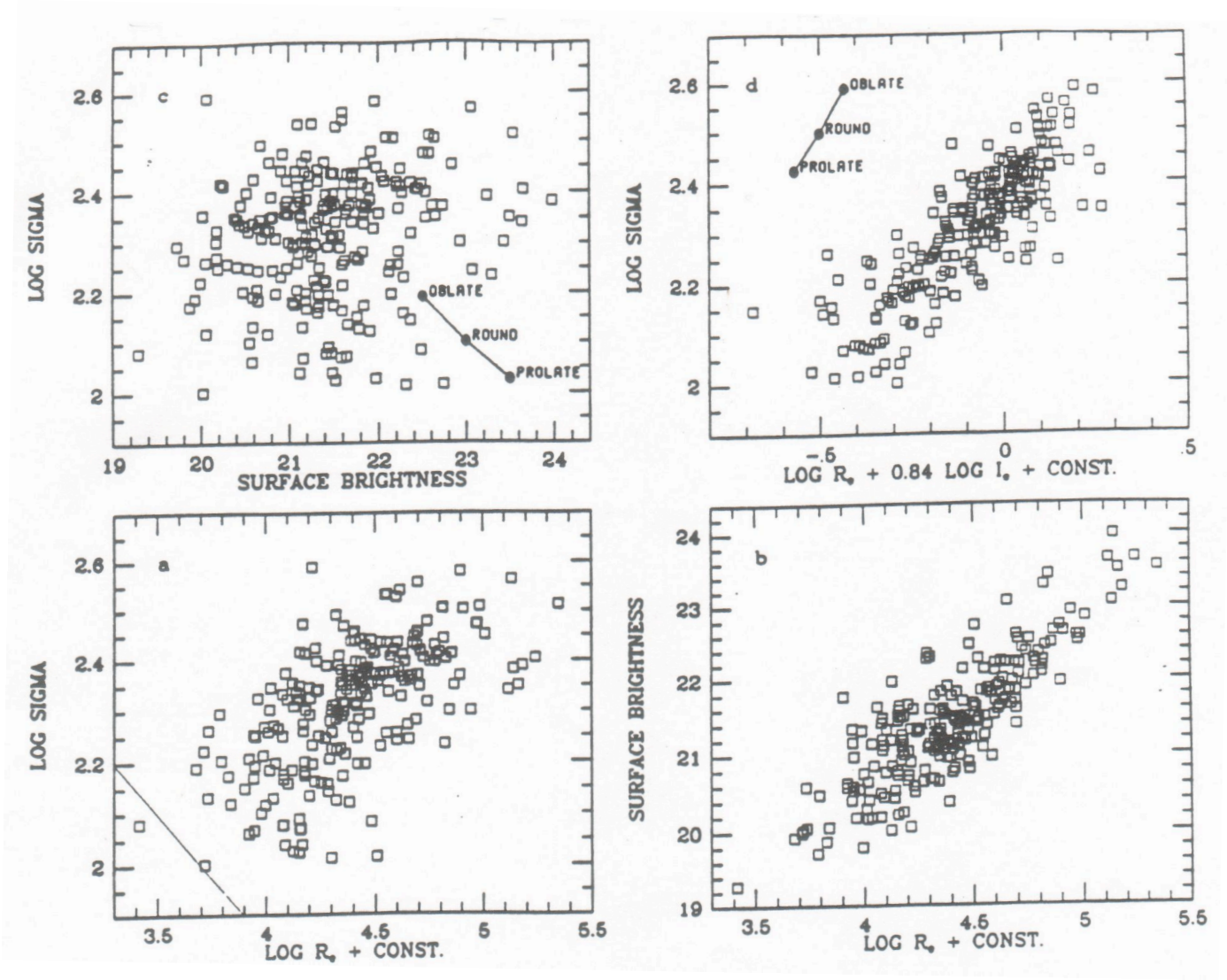

$$r_e \propto \sigma^{1.39} I_e^{-0.90}; \qquad L \propto \sigma^{3.45} I_e^{-0.86}.$$

Fundamental Plane Parameters Determined by Several Different Groups

Figure 1: Structural parameters for our group galaxies. a) Velocity dispersion vs. effective radius. Diagonal line shows constant mass locus. b) Surface brightness vs. effective radius. Shows plane nearly edge-on. c) Velocity dispersion versus surface brightness. Shows plane nearly face-on. Dots show aspect effect on E3.6 oblate and prolate galaxies as seen round and at maximum elongation. d) Velocity dispersion vs. log R_e + 0.84 log I_e. Shows plane exactly edge-on. Dots as in panel c.

The two methods and data sets agree well, as shown in the following table:

Our Group:	R_e	$\sim$	$\sigma_e^{1.35\pm0.07}\ I_e^{-0.84\pm0.03}$
	$(M/L)_e$	$\sim$	$L^{0.24\pm0.04}\ I_e^{\ 0.00\pm0.06}$
DD:	R_e	$\sim$	$\sigma_e^{1.39\pm0.14}\ I_e^{-0.90\pm0.09}$
	$(M/L)_e$	$\sim$	$L^{0.22\pm0.06}\ I_e^{+0.08\pm0.09}$
Lauer (cores):	R_e	$\sim$	$\sigma^{1.48\pm0.21}\ I_c^{-0.84\pm0.09}$
	$(M/L)_e$	$\sim$	$L_c^{0.18\pm0.12}\ I_c^{-0.05\pm0.18}$

3-D View of Fundamental Plane

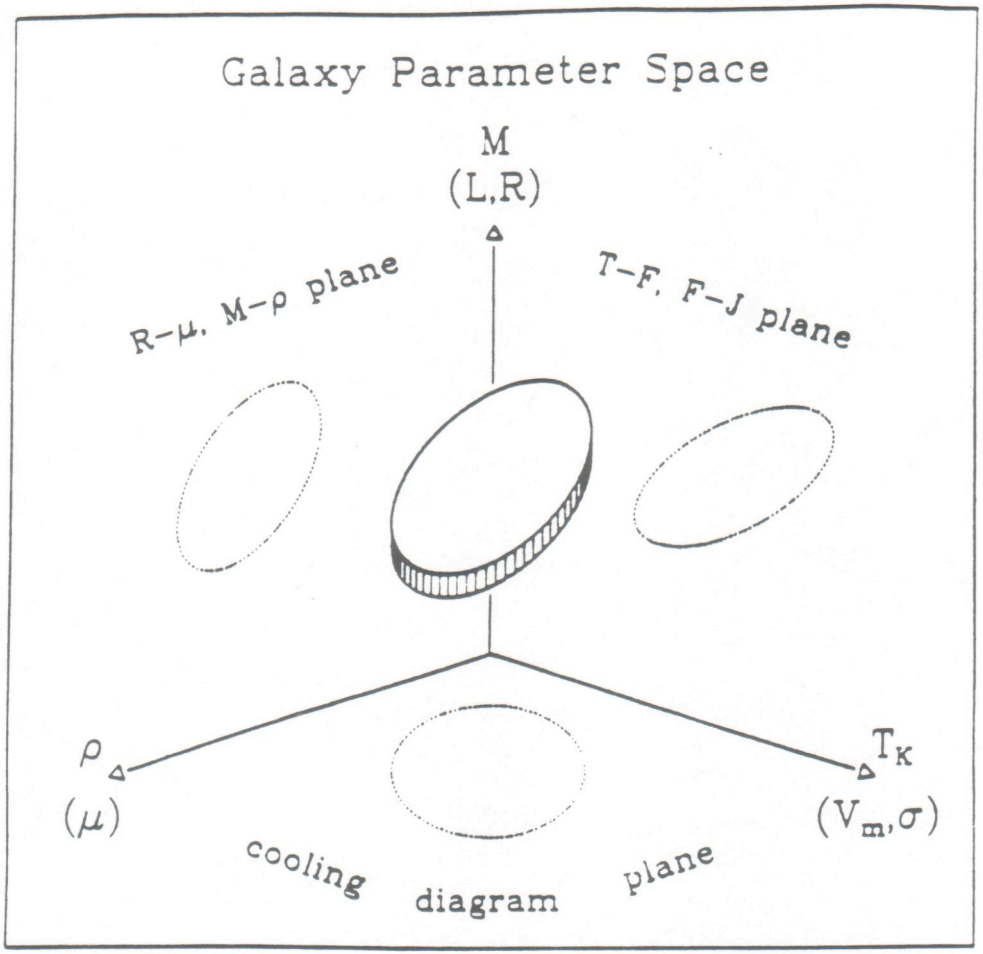

Figure 2. A schematic representation of the galaxy parameter space. Galaxies of a given family (ellipticals or spirals, and probably dwarfs as well) occupy two-dimensional regions (thickened in the third dimension mainly by the measurement errors) in a parameter space whose axes can be called size (mass, luminosity, or radius), density (or surface brightness), and temperature (i.e., kinetic energy per unit mass, typically the maximum rotational velocity for cold disks, or the central velocity dispersion for pressure-supported systems). The particular choice of axes depends on the application and available observables, but the basic picture remains unchanged. The coordinate planes thus defined are some of the well-known diagrams in extragalactic astronomy and cosmology; however, none of them contains all the information, only the oblique projections of the galaxy manifolds.

Fundamental Plane: Some Comments

- If all galaxies are assumed to have the same structure, then the FP is planar only if M / L is a power law in parameters

$$\frac{M}{L} \propto L^n I_e^m,$$

where $n \approx 0.18$ to 0.24 & $m \approx -0.05$ to $+0.08$.

- If the FP seen face-on has no structure, the virial theorem is the only strong constraint
- FP is very narrow & flat , even though data are affected by distance errors, aspect errors, star formation as a result of merging, etc.

Fundamental Plane: Some Comments (cont')

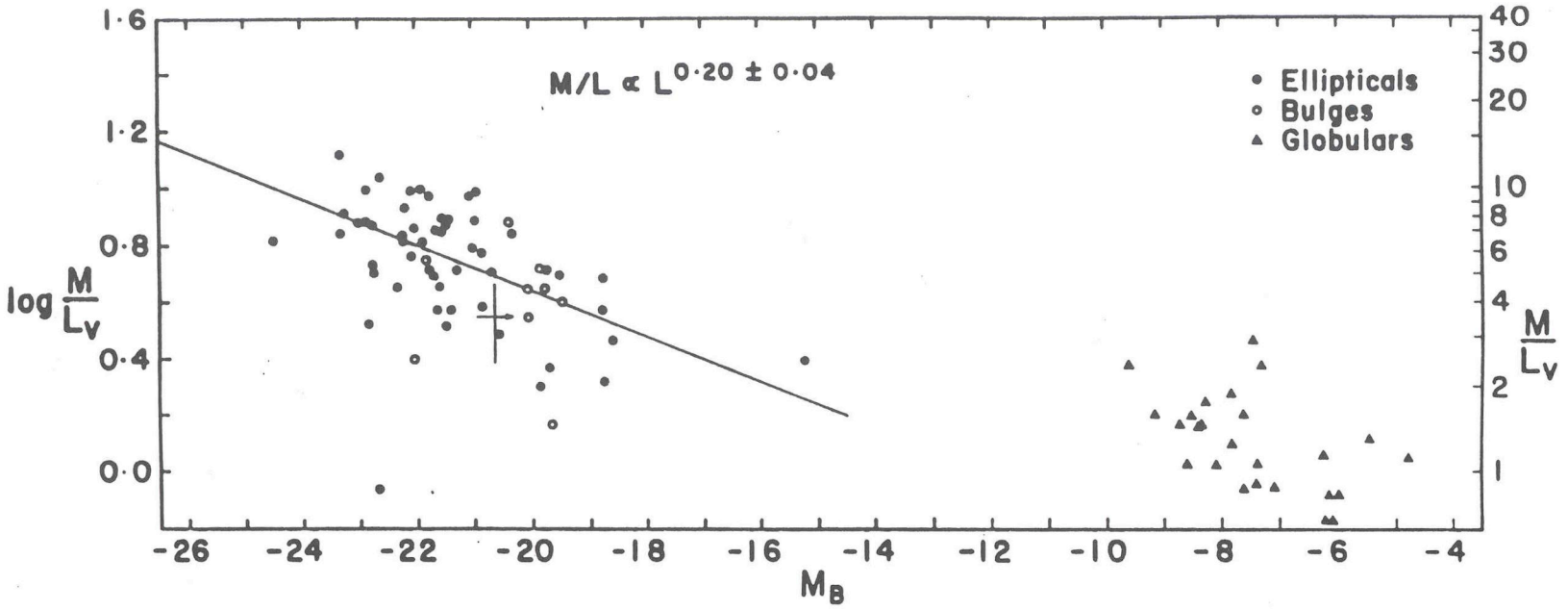

Fig. 8. – Core mass-to-light ratios for bulges, elliptical galaxies and globular clusters (Kormendy 1987b). The line is a least-squares fit to the ellipticals. The plus sign is the mean M/L_V for old disks; the error bar is the dispersion of values seen (Kormendy 1987a).

- *M / L* vs. *L* relation has very little scatter (i.e., 16%), which indicates that stellar populations are very homogeneous. Thus,

$$\frac{M}{L} \sim L^{0.20}.$$

Fundamental Plane: Some Comments (cont')

- Core & global parameters give very similar results

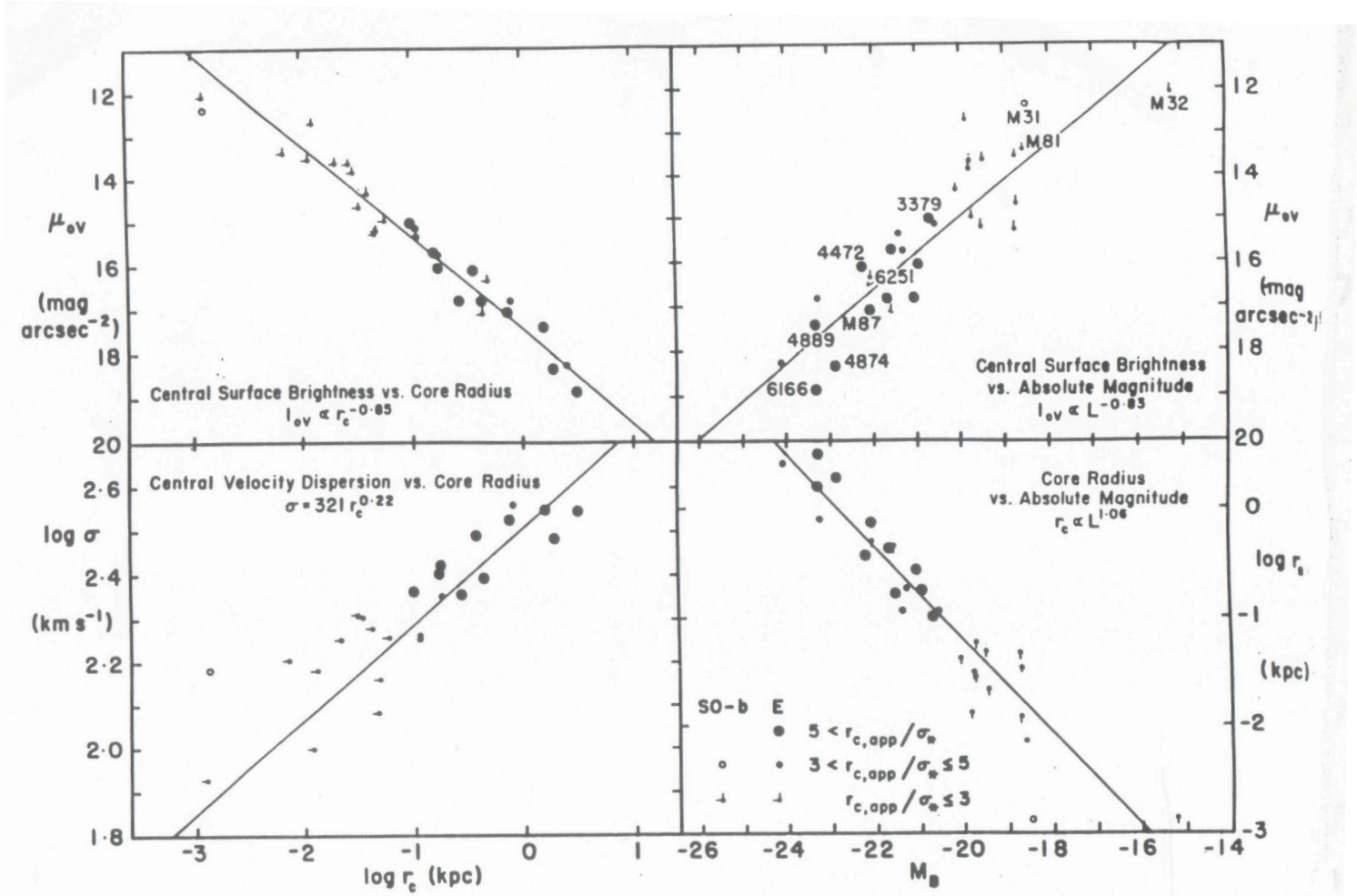

FIG. 2.—Core parameter relations for bulges and elliptical galaxies. Several points are labeled with corresponding NGC or Messier numbers. Open circles for bulges are derived using all of the observed profile, including any nucleus. The straight lines are least-squares fits to the data for elliptical galaxies. M32 is omitted from the regressions because it may be tidally truncated by M31 and hence too faint for its core parameters.

Core Parameters

- Core radius, r_c, is the radius at which the projected surface brightness is half its central brightness
- If M / L = constant, the ρ / I = constant. Thus,

$$\rho \propto I.$$

- The projected profile is,

$$\rho(r) = \frac{\rho_0}{1 + \left(\frac{r}{r_c}\right)^2}.$$

- Note that when $r = r_c$, $\rho\ (r_c) = 0.5\rho_0$. Also, for $r >> r_c$,

$$\rho(r) \propto r^{-2}.$$

- The unprojected profile is,

$$\rho(r) = \frac{\rho_0}{\left[1 + \left(\frac{r}{r_c}\right)^2\right]^{3/2}}.$$

- We want to solve Poisson's equation using the unprojected density equation given above. Using the distribution function for an isothermal sphere,

$$f(\epsilon) = \frac{\rho_0}{(2\pi\sigma^2)^{3/2}} e^{\epsilon/\sigma^2},$$

where $\epsilon = \Phi - (1/2)v^2$

$$\rho = \int_0^\infty f(\epsilon) d^3v = \rho_0 e^{\Phi/\sigma^2},$$

Solving for potential,

$$\Phi = \sigma^2 \ln\left[1 + \left(\frac{r}{r_c}\right)^2\right]^{-3/2}.$$

Poisson's Equation,

$$\nabla^2\Phi = -4\pi G\rho,$$

Can be expressed in spherical coordinates as,

$$\nabla^2\Phi = \frac{1}{r^2}\frac{d}{dr}\left[r^2\frac{d\Phi}{dr}\right] = \frac{2}{r}\frac{d\Phi}{dr} + \frac{d^2\Phi}{dr^2} = -4\pi G\rho.$$

At $r = 0$, Poisson's Equation becomes,

$$\frac{2}{r}\frac{d\Phi}{dr} + \frac{d^2\Phi}{dr^2} = -\frac{6\sigma^2}{r_c^2} - \frac{3\sigma^2}{r_c^2} = -\frac{9\sigma^2}{r_c^2} = -4\pi G\rho_0.$$

Solving for r_c yields,

$$r_c = \left[\frac{9\sigma^2}{4\pi G\rho_0}\right]^{1/2},$$

$$r_c = \left[\frac{9\sigma^2}{4\pi G\rho_0}\right]^{1/2},$$

In terms of density,

$$\rho_0 = \frac{9\sigma^2}{4\pi G r_c^2}.$$

The *M / L* ratio is defined in terms of core parameters by First taking the central luminosity density j_0 to be,

$$j_0 = \frac{(1/2)I_0}{r_c}.$$

Thus,

$$\left(\frac{M}{L}\right)_c = \frac{\rho_0}{j_0} = \frac{9\sigma^2}{2\pi G I_0 r_c}$$

Ordered vs. Random Motion – the v / σ Diagram

$\sigma_z = \sigma_r = \sigma_\theta$

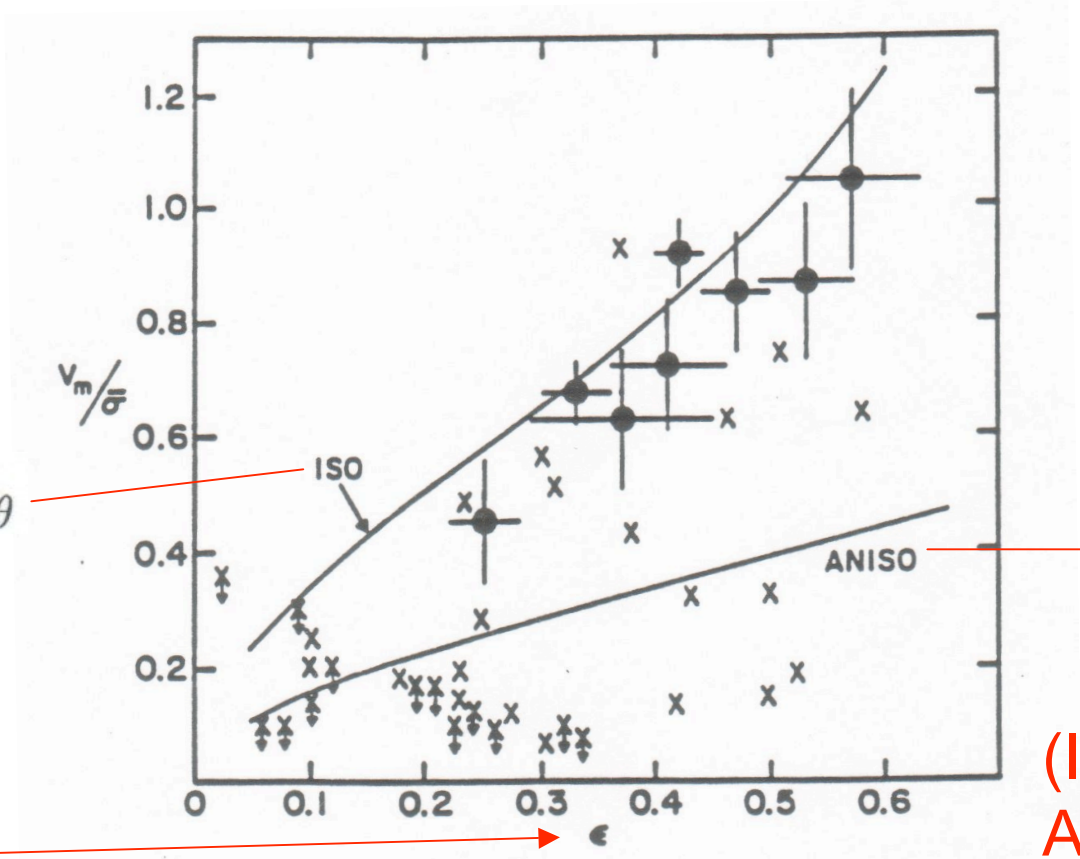

$\sigma_z < \sigma_r, \sigma_\theta.$

$\epsilon = 1 - \frac{b}{a},$

FIG. 3.—Comparison of bulge data (*filled circles*) with all available elliptical galaxy data (*crosses*, *arrows* indicate upper limits) in the dimensionless rotation-ellipticity plane. Derivation of V_m, $\bar{\sigma}$, and ϵ is discussed in the text. The line labeled ISO represents projected models of oblate spheroids with isotropic residual velocities and rotational flattening. The line labeled ANISO describes a typical anisotropic oblate model with σ_z smaller than σ_r and σ_θ.

(Illingworth 1977 ApJ, 218, L43; Davies et al. 1983, ApJ, 266, 41)

b = semi-major axis, *a* = semi-minor axis

v/σ Diagram

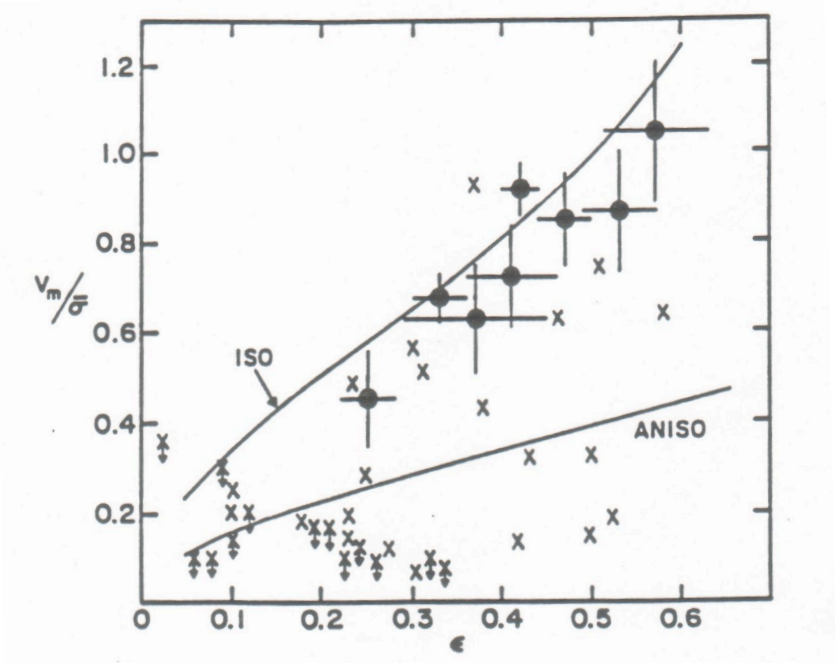

FIG. 3.—Comparison of bulge data (*filled circles*) with all available elliptical galaxy data (*crosses*, *arrows* indicate upper limits) in the dimensionless rotation-ellipticity plane. Derivation of V_m, $\bar{\sigma}$, and ϵ is discussed in the text. The line labeled ISO represents projected models of oblate spheroids with isotropic residual velocities and rotational flattening. The line labeled ANISO describes a typical anisotropic oblate model with σ_z smaller than σ_r and σ_θ.

- Bulges of spirals & faint elliptical galaxies lie close to the ISO line
- Brighter elliptical galaxies lie near ANISO line

Key Points about Ellipticals and Bulges

- Low luminosity ellipticals & bulges
    1) Rotate rapidly
    2) Have nearly isotropic σ
    3) Are flattened by rotation
- Bright Ellipticals
    1) Rotate slowly
    2) Are pressure supported
    3) Have shapes due to velocity anisotropy

Boxy vs. Disky Isophotes

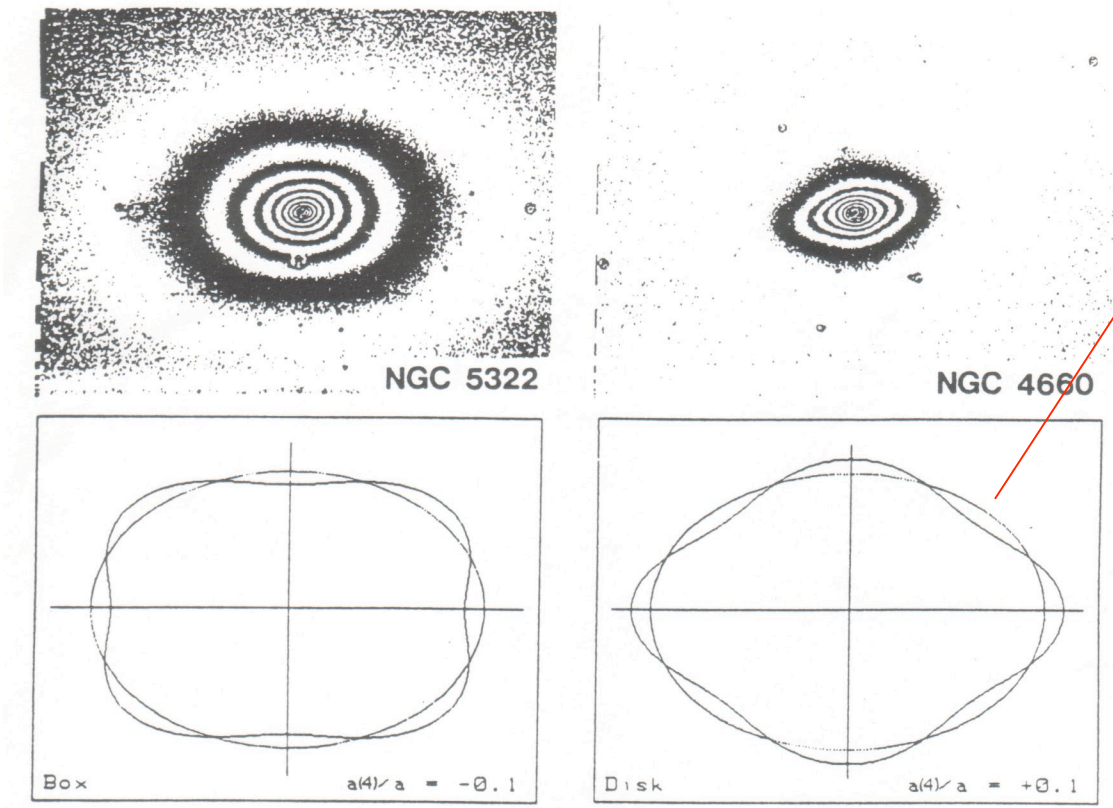

Isophote for ellipse r_{ell} (θ), where θ = polar angle.

(Bender et al. 1988, A&AS, 74, 385)

Departure from Ellipse → $$r - r_{\rm ellipse} = \sum_{n=3}^{?} a_n \cos n\theta + \sum_{n=3}^{?} b \sin n\theta,$$

$a_4 < 0 \rightarrow$ box − shaped isophotes

$a_4 > 0 \rightarrow$ disk − shaped isophotes

← Most significant term

Boxy vs. Disky Isophotes

- Elliptical galaxies with boxy isophotes have anisotropic σ
- Elliptical galaxies with disky isophotes are rotationally flattened & have isotropic σ

Boxy vs. Disky Isophotes

$$v/\sigma_* = \frac{(v/\sigma)_{\rm observed}}{(v/\sigma)_{\rm ISO}}$$

- Anisotropic galaxies have v / σ_* < 1.

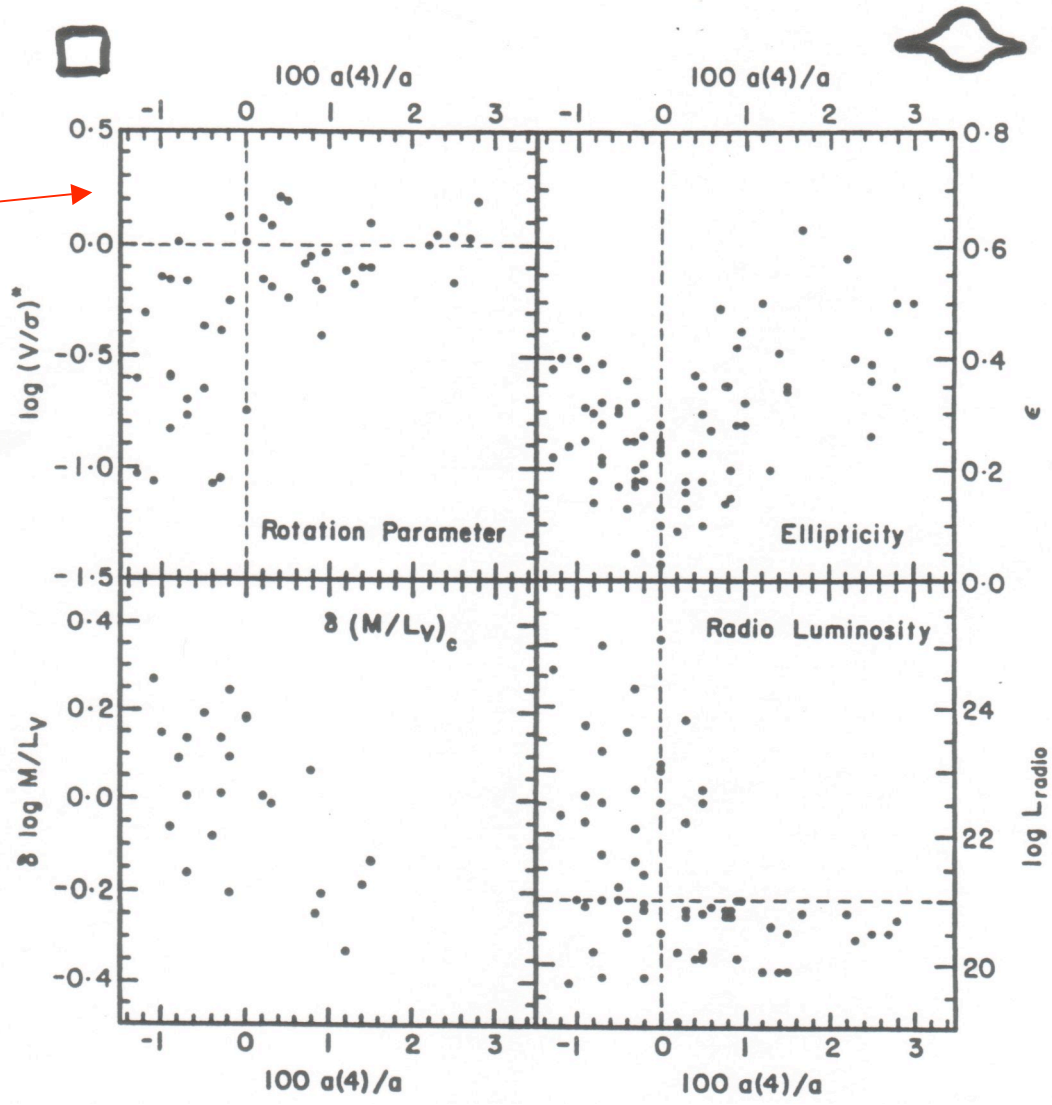

(Bender et al. 1989, A&A, 217, 35; Kormendy & Djorgovski 1989 ARAA, 27, 35)

HST Observations of Elliptical Cores & Bulges

- Luminous hot galaxies ($M_V < -22$)
    1) Cuspy Cores
    2) Boxy & Slowly Rotating
    3) Relatively low density, large cores
- Intermediate hot galaxies ($-22 < M_V < -20.5$)
    1) Mix of core & power-law galaxies
- Faint hot galaxies ($M_V > -20.5$)
    1) Power Law profiles that lack cores
    2) Disky & rapidly rotating
    3) 1000 times denser in mass & luminosity than cores of large galaxies

(This later group includes M32, small Virgo ellipticals & spiral bulges)

Break Radius

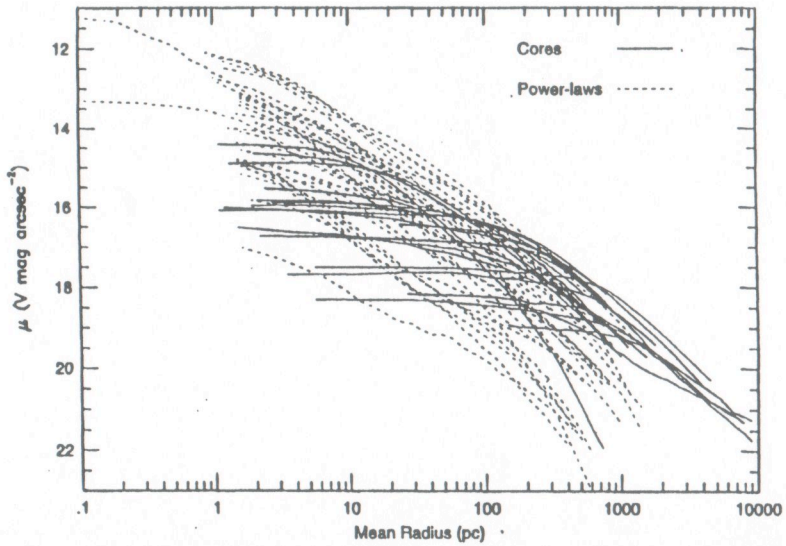

FIG. 1. *V*-band surface-brightness profiles of 55 ellipticals and bulges from *HST*. All were observed in the WFPC1 Planetary Camera through filter F555W and were deconvolved using the Lucy-Richardson algorithm as described in Paper I. Core galaxies (see Sec. 2) are plotted as solid lines, and power-law galaxies are plotted as dashed lines. "Mean radius" is the geometric mean of the semimajor and semiminor axes of the isophotal ellipse.

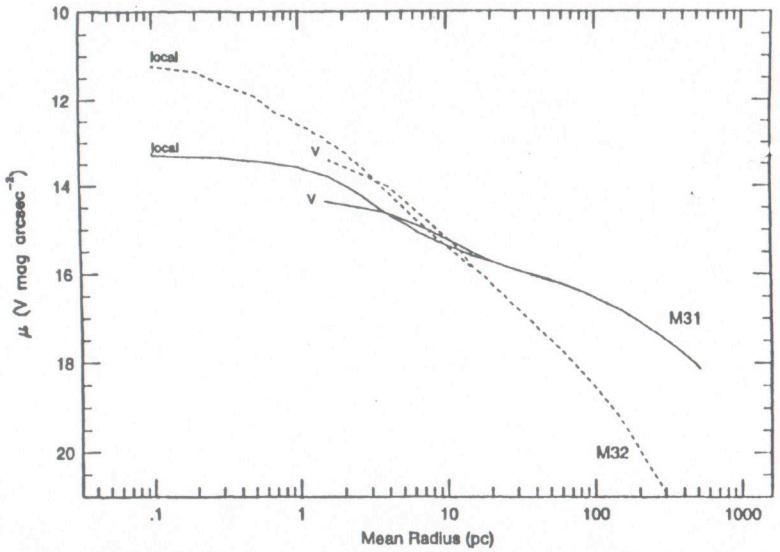

FIG. 2. *HST* surface-brightness profiles of M31 and M32, as seen locally and near Virgo (24 times farther). To simulate Virgo, the nearby profile was binned by a factor of 24, convolved with the WFPC1 point-spread function, and deconvolved with 80 iterations of the Lucy–Richardson algorithm.

r_b: the point of maximum curvature in the surface brightness profile plot.

The slope, γ, is defined as,

$$\gamma = -\frac{d \log I}{d \log r}.$$

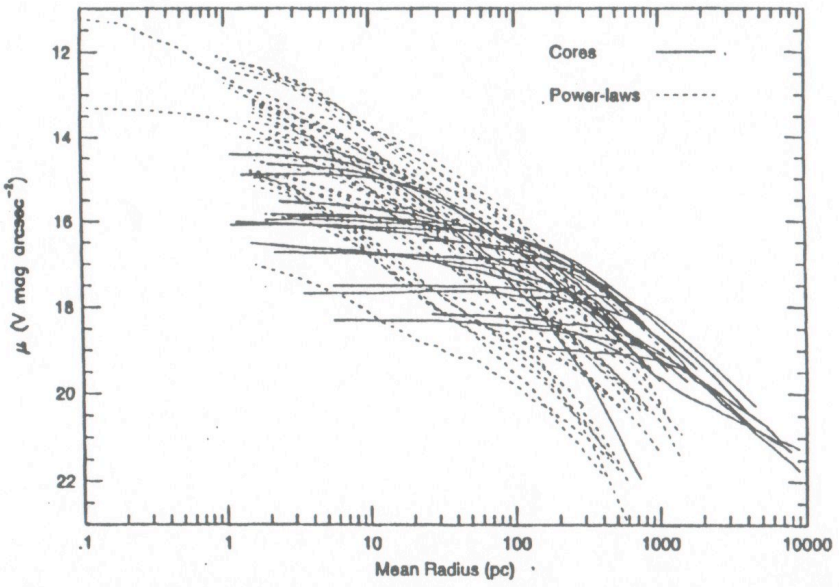

FIG. 1. *V*-band surface-brightness profiles of 55 ellipticals and bulges from *HST*. All were observed in the WFPC1 Planetary Camera through filter F555W and were deconvolved using the Lucy-Richardson algorithm as described in Paper I. Core galaxies (see Sec. 2) are plotted as solid lines, and power-law galaxies are plotted as dashed lines. "Mean radius" is the geometric mean of the semimajor and semiminor axes of the isophotal ellipse.

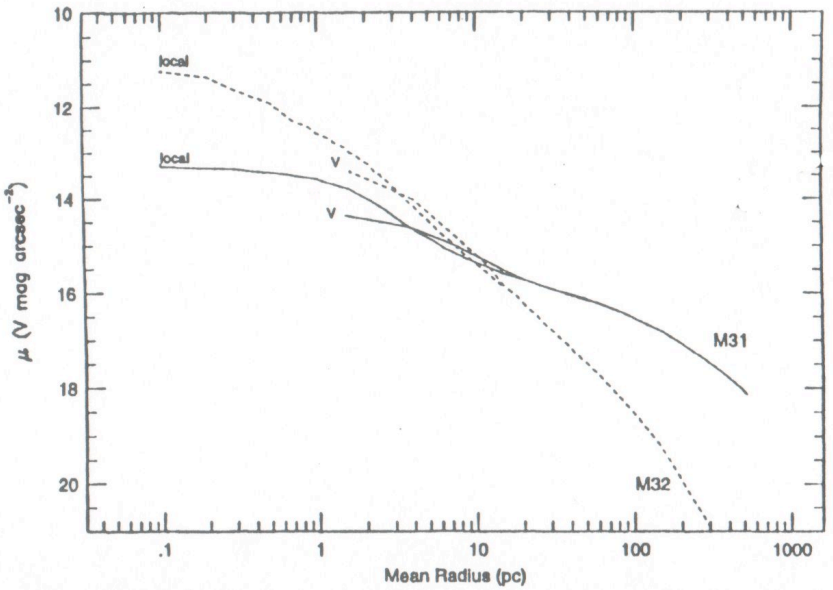

FIG. 2. *HST* surface-brightness profiles of M31 and M32, as seen locally and near Virgo (24 times farther). To simulate Virgo, the nearby profile was binned by a factor of 24, convolved with the WFPC1 point-spread function, and deconvolved with 80 iterations of the Lucy–Richardson algorithm.

Nuker Law,

$$I(r) = I_b 2^{(\beta-\gamma)/\alpha} \left(\frac{r_b}{r}\right)^{\gamma} \left[1 + \left(\frac{r}{r_b}\right)\right]^{(\gamma-\beta)/\alpha}$$

– γ = slope inside r_b

– β = slope outside r_b

α = sharpness of break

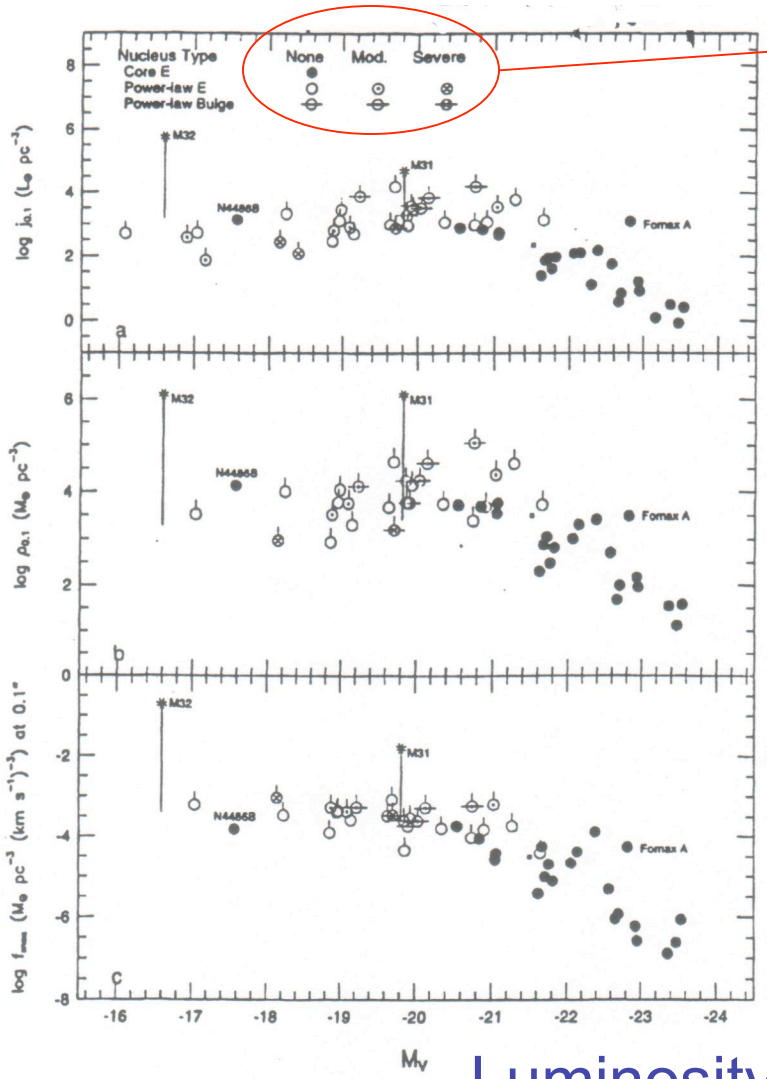

FIG. 6. Various densities at radius 0.1 plotted against absolute magnitude. Mass densities are derived by normalizing nuker-law surface-brightness fits to central σ_0. The symbols are the same as in Fig. 4. Model details are given in the text and notes to Table 3. Panel (a) luminosity density; panel (b) mass density; panel (c) peak Maxwellian phase-space density. Note the range of almost 10^6 in density in all three panels. Turndowns for small galaxies are probably an artifact of resolution (cf. M32).

Degree of Nucleation

Luminosity Density

Mass Density

Phase-Space Density, $f \sim \rho\, \sigma^{-3}$

Luminosity →

Note the range in density

Break Radius

Velocity Disper-sion

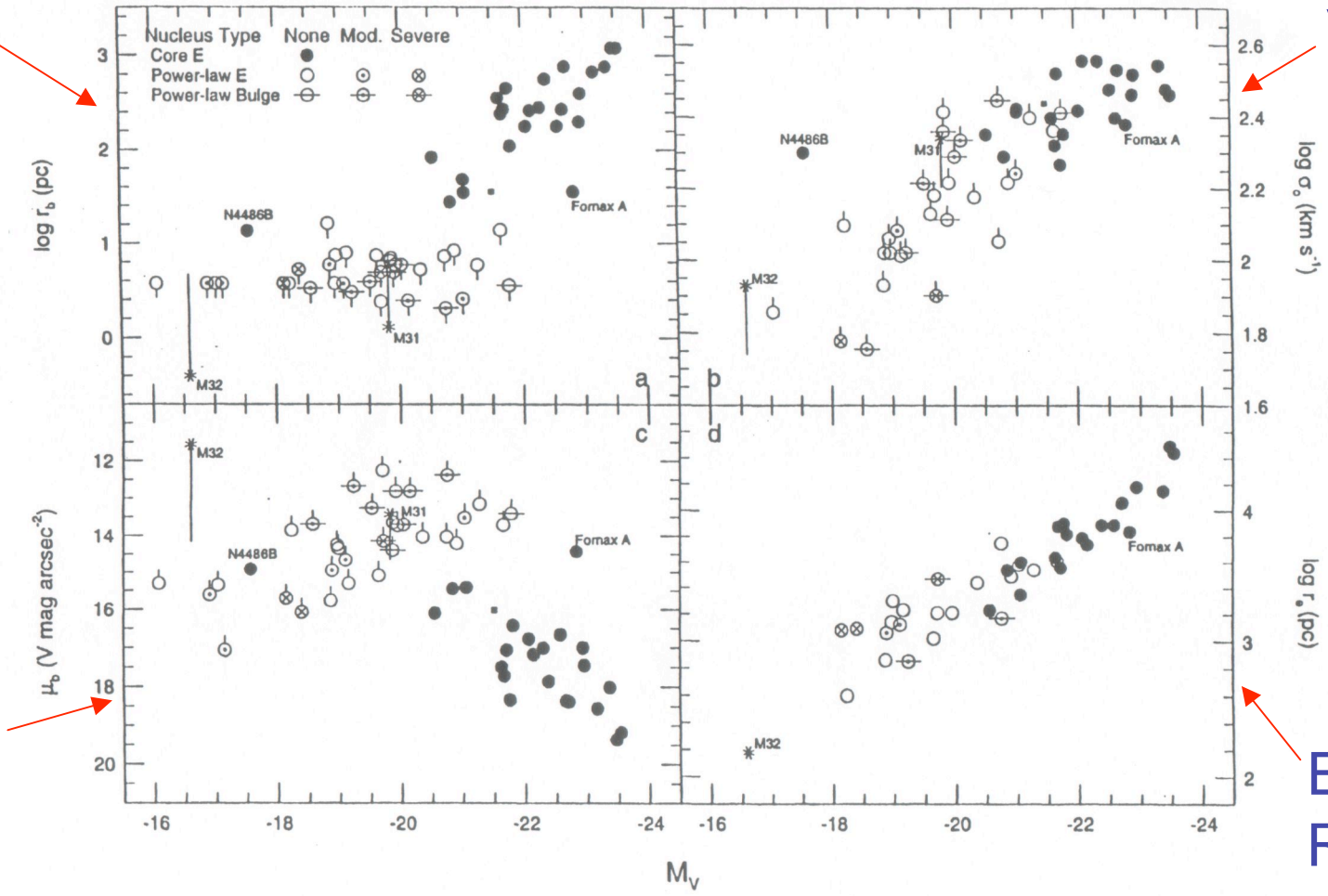

Surface Bright-ness

Effective Radius

FIG. 4. *HST* measurements of central parameters of hot galaxies, as a function of absolute V magnitude. Hubble type and nucleus types are taken from Table 1; "bulges" are S0-Sb galaxies. r_b and μ_b for power laws are limits $r_b^{\lim}$ and $\mu_b^{\lim}$ from Table 2. M31 and M32 are plotted twice: asterisks show data as observed, and tails indicate their positions as they would appear 24 times farther away near Virgo. The small black square is the S0 galaxy NGC 524, which is the only core within a bulge. The apparent turndown in surface brightness at faint magnitudes in panel (c) is probably a resolution effect (cf. M32). Effective radii are plotted in panel (d), to be compared with break radii in panel (a): the strong impressions of scatter at intermediate magnitudes ($-22 < M_V < -20.5$) and of two types of galaxies in panel (a) are absent in panel (d).

More trends with Luminosity…

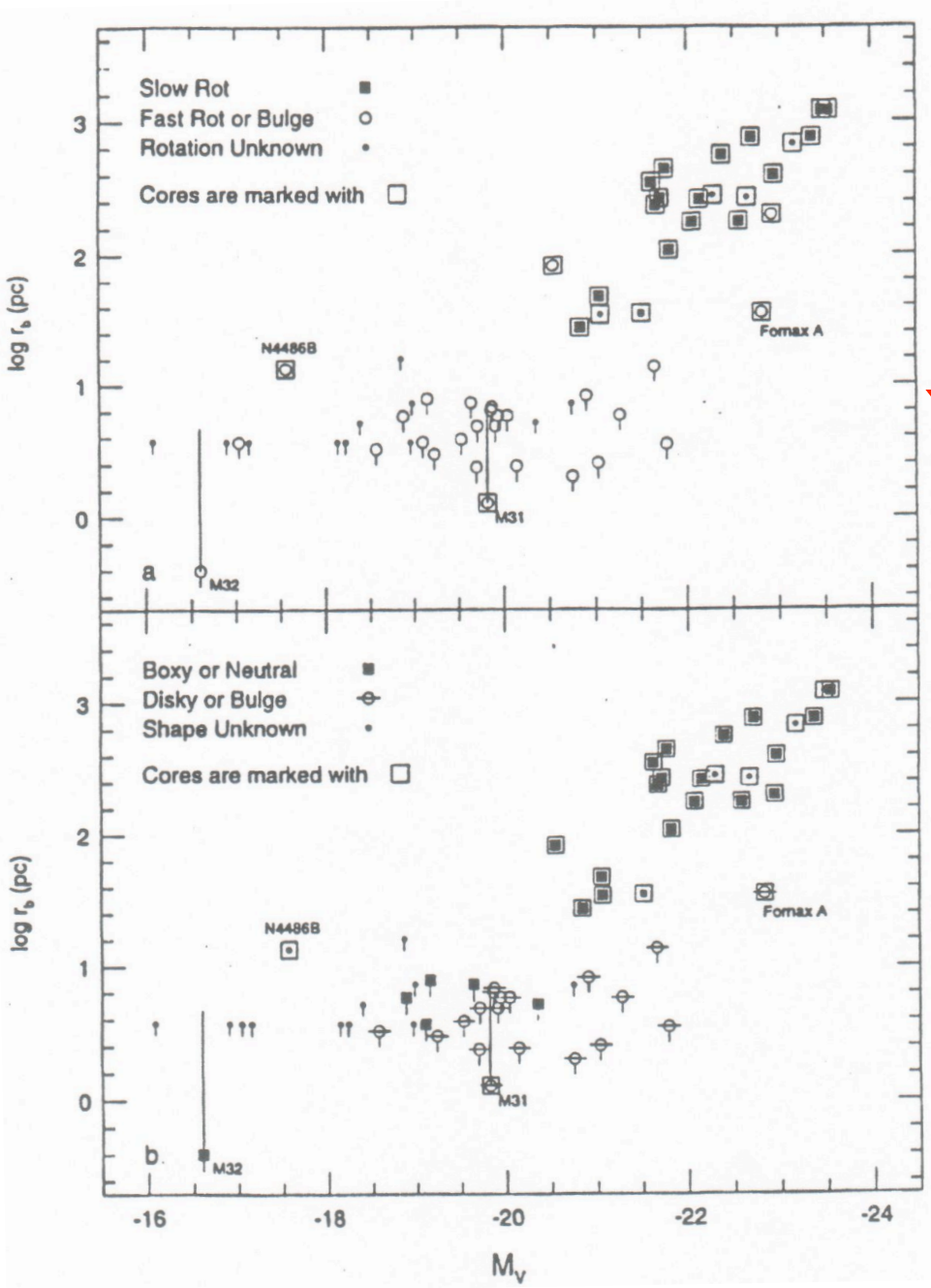

FIG. 7. (a) Replot of Fig. 4(a) with symbols indicating rotation speed $(v/\sigma)_*$. Slow rotators (filled symbols) have $(v/\sigma)_* < 0.51$; fast rotators (open circles) have $(v/\sigma)_* \geq 0.51$. Bulges lacking data are classed as fast rotators. Galaxies with core profiles are indicated by the enclosing squares; all others are power laws. The data indicate a tendency for fast rotators to have power-law profiles. (b) Same as (a) but with symbols indicating isophotal shape a_4/a. Galaxies are classed as disky if $a_4/a \geq 0.4$, otherwise as boxy/neutral. Irregular profiles with variable a_4/a are also classed as boxy/neutral. Bulges (Hubble types S0-Sb) are classed as disky. The data indicate a tendency for disky galaxies to have power-law profiles.

"Slow vs. Fast Rotation"
v / σ

"Boxy vs. Disky"
a_4 / a

Trends with Luminosity…

Core Fundamental Plane

A core FP can exist only if the cores are:

- In dynamic equilibrium
- Random motions are significant
- Anisotropies do not vary much from galaxy to galaxy
- M / L is a function of μ_b, r_b, & σ_0

For cores,

$$\log \sigma = 0.766 \log r_b - 0.257 \mu_0 + 2.97$$

Fundamental Planes for “Cores”

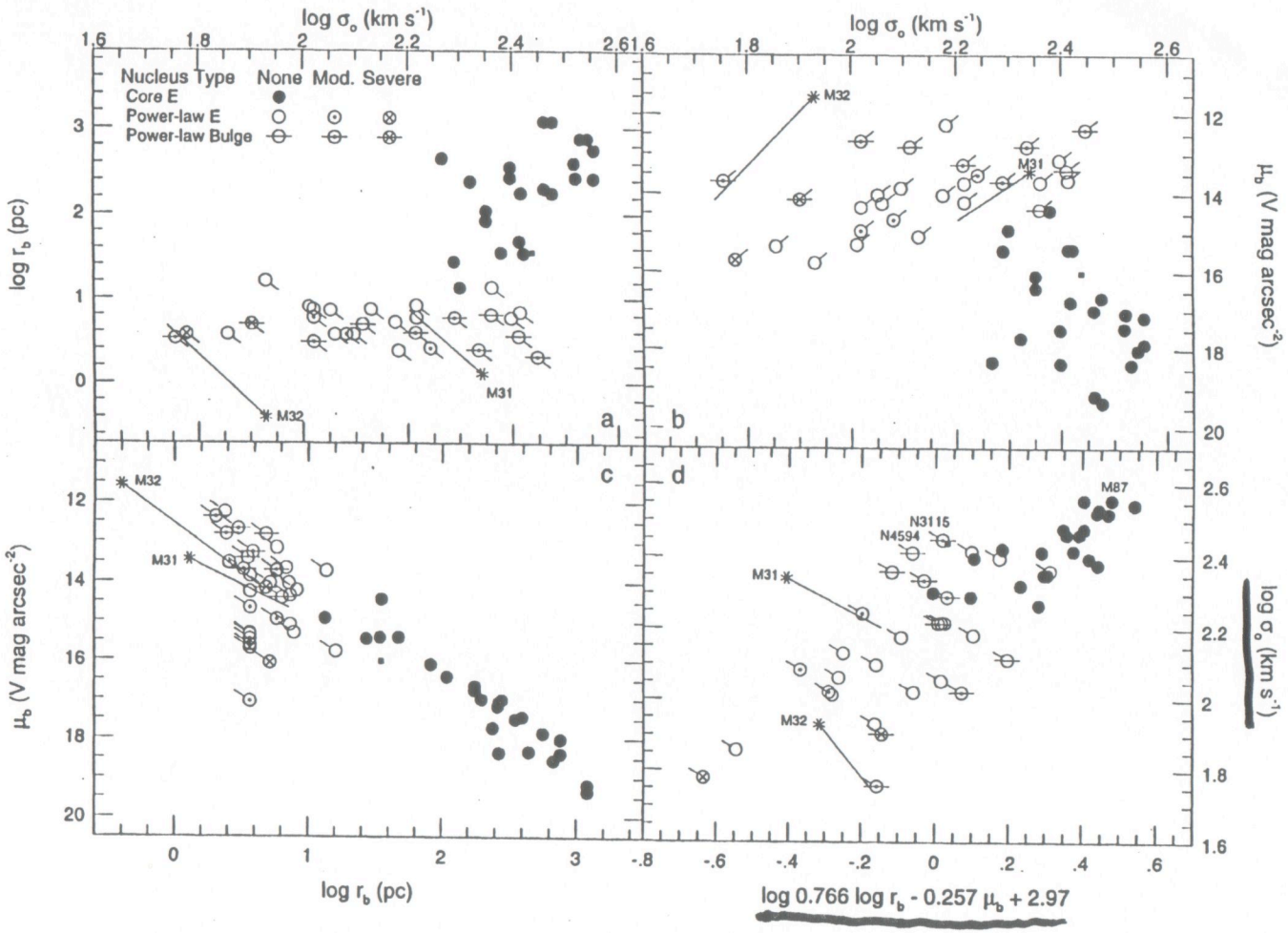

FIG. 8. *HST* measurements of central parameters of hot galaxies in fundamental-plane space. Symbols are the same as in Fig. 4. Tails on M31 and M32 (asterisks) show the effect of moving these galaxies 24 times further away to the vicinity of Virgo. Resolution effects on other power-law galaxies may be similar and are indicated schematically by the limit flags. Panel (d) shows the fundamental plane rotated about the σ_0 axis and viewed edge-on (for cores). The rotation chosen uses the same power-law combination of r_b and I_b used for the global fundamental plane of elliptical galaxies by Faber *et al.* (1987) and is consistent with their best core plane within the statistical errors. The rms scatter about the central plane (cores only) is 0.12 dex, which is 50% greater than the scatter about the global plane. This increase may be due in part to the influence of central BHs on σ_0. Five BH candidates from Kormendy & Richstone (1995) are marked in panel (d).

Core Fundamental Plane (cont')

- The scatter in the core FP is 30% larger than that of the global (effective radius) FP.
- A possible explanation is the supermassive black hole in some of the galaxies may heat the core, causing the σ to be higher
- Note that in σ vs. $0.766 \log r_b - 0.257\mu_0 + 2.97$ plot, the upper σ envelope is comprised of galaxies with strong evidence of supermassive nuclear black holes.

The tightness of the core FP is surprising given that

- Profiles differ (i.e., α & γ vary)
- Anisotropy may vary from galaxy to galaxy
- Some have black holes that affect the $I(r)$ and σ
- Core are only a small fraction of the total luminosity of the galaxies

Why do some Ellipticals have Large Cores whereas others do not?

- Power-law nuclei, which high phase-space densities, may be created by galaxy-galaxy mergers

$$f \propto \frac{\rho}{\sigma^3}$$

- Core nuclei, which are associated with large ellipticals, may be created in part by the slow accretion of satellite galaxies (via dynamical friction)

The following is a set of self-consistent scaling relations versus L_V and galaxy mass, $\mathscr{M}$. Total luminosity has been related to mass by assuming $(\mathscr{M}/L_V) \propto L^{0.25}$ (Faber *et al.* 1987). The exponents in these relations are not least-squares fits but have been derived by a process of trial-and-error adjustment to maintain consistency with standard structural formulas. The first three of these relations are independent fits to the data, while the rest are derived from the structural formulas. The relations involving $\mathscr{M}_{\rm core}$ assume that the core is in dynamical equilibrium:

$$r_b \propto L_V^{1.15} \propto M^{0.92}, \tag{3}$$

$$I_b \propto L_V^{-1.0} \propto M^{-0.8}, \tag{4}$$

$$\sigma_0 \propto L_V^{0.2} \propto M^{0.16}, \tag{5}$$

$$j_{\rm core} \sim \frac{I_b}{r_b} \propto L_V^{-2.15} \propto M^{-1.72}, \tag{6}$$

$$L_{\rm core} \sim I_b r_b^2 \propto L_V^{1.3} \propto M^{1.04}, \tag{7}$$

$$\mathscr{M}_{\rm core} \sim \sigma_0^2 r_b \propto L_V^{1.55} \propto M^{1.24}, \tag{8}$$

$$\mathscr{M}_{\rm core}/L_{\rm core} \sim \frac{\sigma_0^2}{I_b r_b} \propto L_V^{0.25} \propto M^{0.2}, \tag{9}$$

$$\rho_{\rm core} \sim \frac{\sigma_0^2}{r_b^2} \propto L_V^{-1.9} \propto M^{-1.52}. \tag{10}$$

Elliptical Galaxies: Remaining Issues (for now)

- Does the Fundamental Plane Hold at Higher z?
- The Interstellar Medium of Elliptical Galaxies?

Fundamental Plane for z = 0.33 Cluster Cl 1358+62

- 30 E and S0 galaxies
- Log r_e ~ 1.31±0.13 log σ – 0.86±0.10 log I_e
- Scatter in M / L_V is 14%
- Thus, E and S0 galaxies are structural mature by this redshift

- This values are similar to the FP values of the Coma Cluster
- E.g., log r_e ~ 1.24 log σ – 0.82 log I_e

(Kelson et al. 2000; van Dokkum 1998)

FIG. 2.—Color representation of the central part of Fig. 1, created from the F606W and F814W exposures. The cluster members are easily recognized by their yellow colors. However, many of the bluer galaxies are also cluster members.

(van Dokkum 1998)

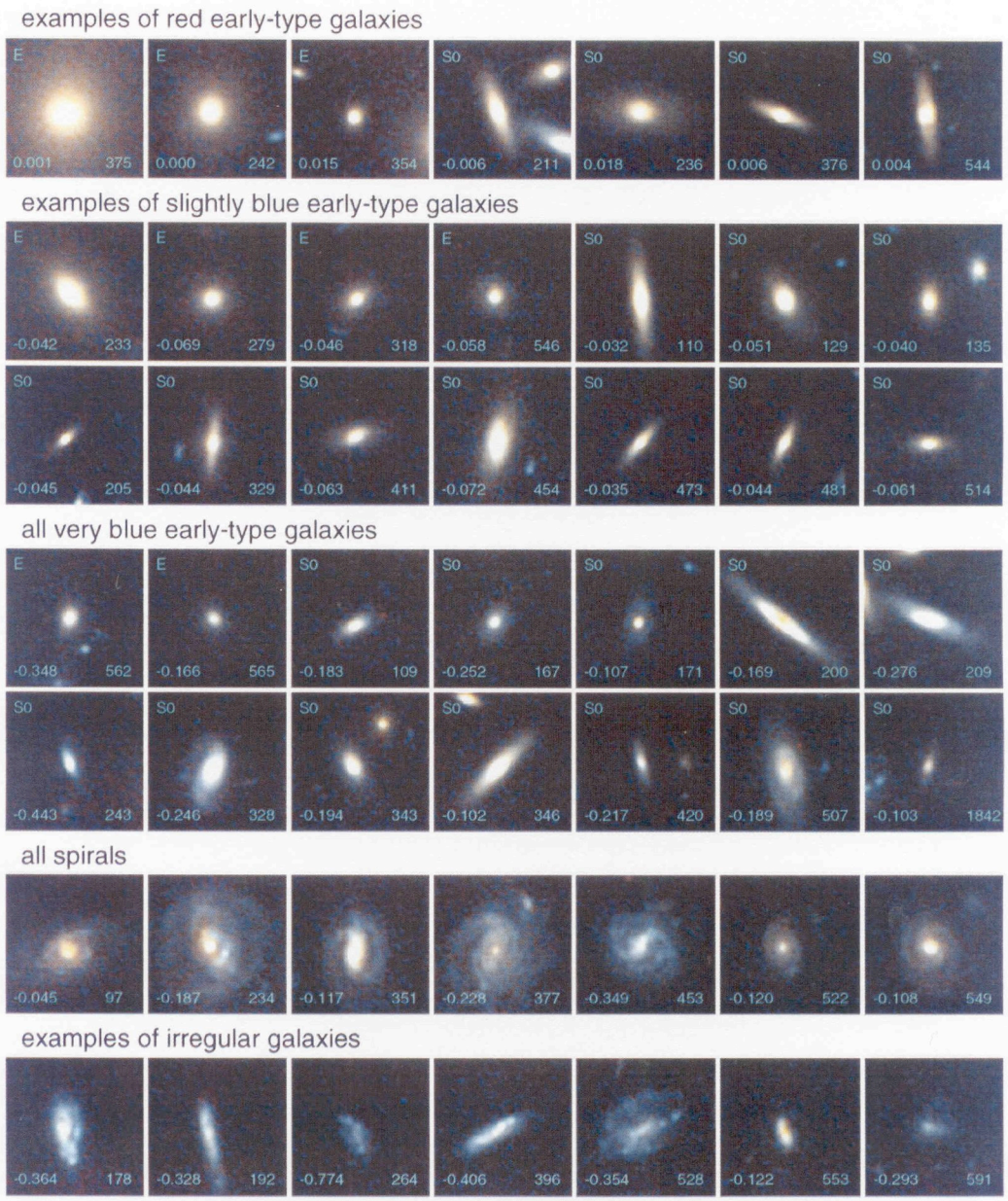

FIG. 4.—Examples of early-type galaxies on the CM relation, examples of slightly blue early types, all very blue early types, all spirals, and examples of irregular galaxies. Each box is 6.″4 × 6.″4 (37 × 37 h_{50}^{-1} kpc). The number in the lower right of each box is the galaxy identification, and the number in the lower left is the rest-frame $B-V$ color with respect to the CM relation. The slightly blue early-type galaxies have very similar morphologies to the early types on the CM relation. The very blue early types have low luminosities and generally have significant disks.

(van Dokkum 1998)

Fundamental Plane at Intermediate z

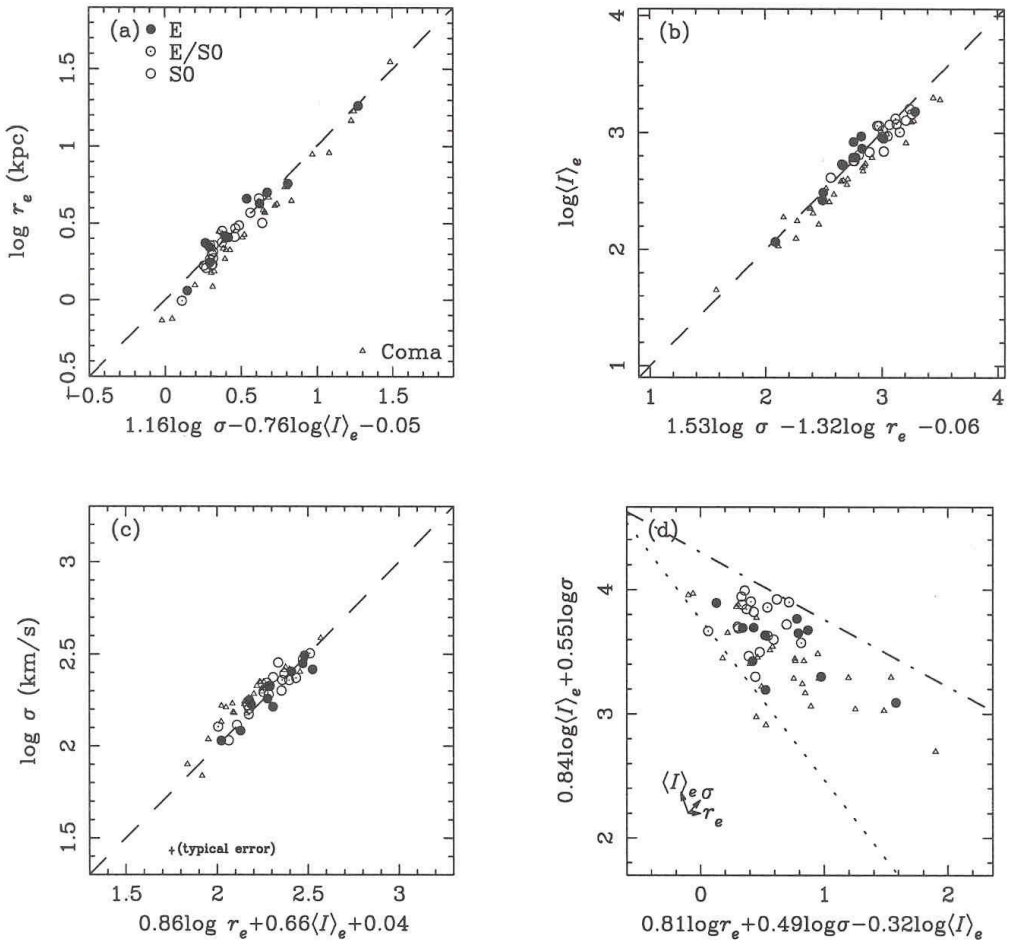

FIG. 1.—Fundamental plane of early-type galaxies in Cl 1358+62, showing the (*a*) long, (*b*) intermediate, and (*c*) short edge-on views and (*d*) the face-on distribution. The early-type galaxies clearly form a tight relation in (*a*–*c*). The dashed lines show the fit to the elliptical galaxies of Cl 1358+62. In (*c*), we show the size of a typical error. The absence of galaxies in the lower left region of (*d*) is attributed to the magnitude limit of the sample (*dotted line*). The absence of galaxies in the upper right is referred to as the zone of avoidance (Bender et al. 1993). The Cl 1358+62 galaxies are shown by the large symbols indicated in (*a*). The Coma *V*-band sample is shown by small triangles (Jørgensen et al. 1996).

(Kelson et al. 2000)

FP at Intermediate z, cont.

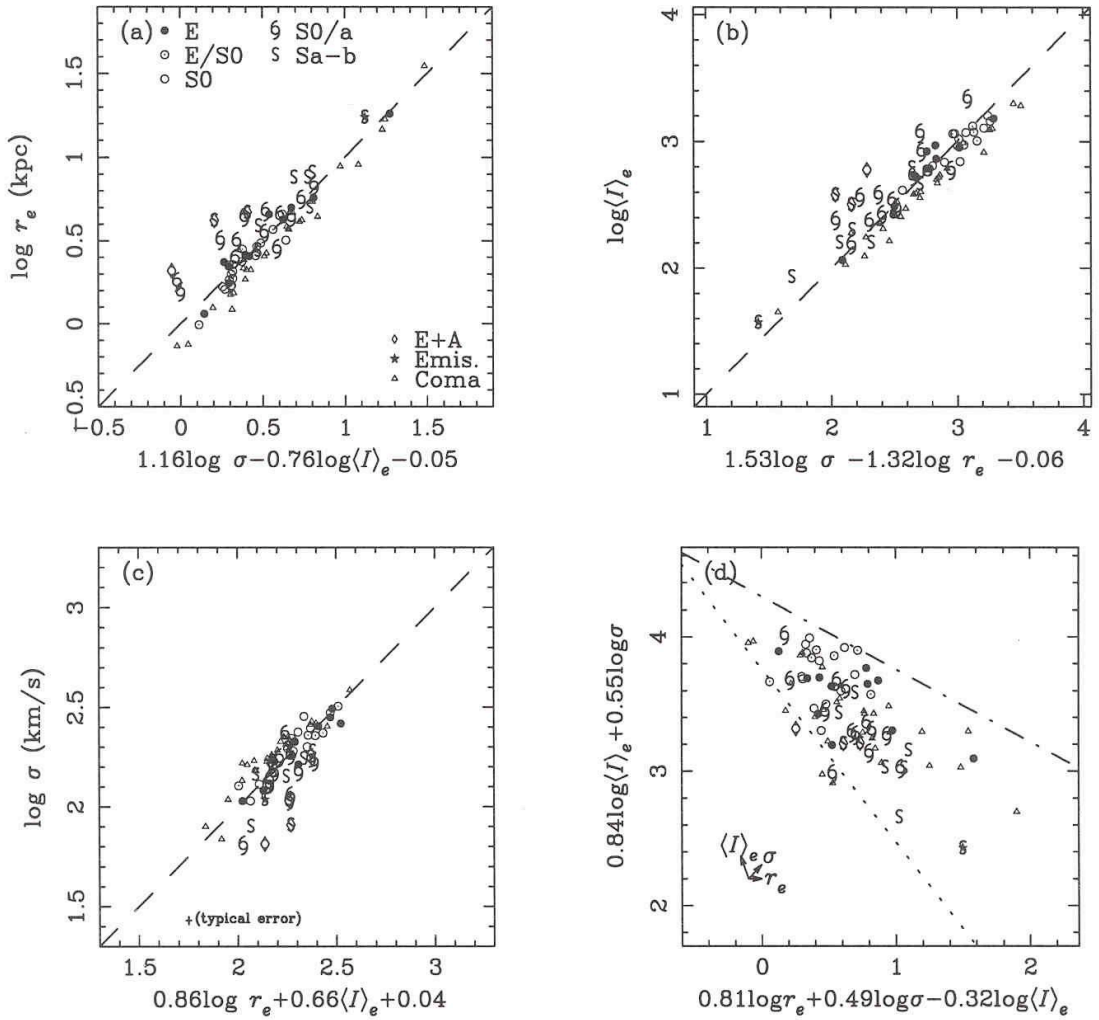

FIG. 4.—Full sample of 53 galaxies shown together. Note that the later type galaxies are systematically brighter than the plane of the early types.

(Kelson et al. 2000)

FP at Intermediate z, cont.

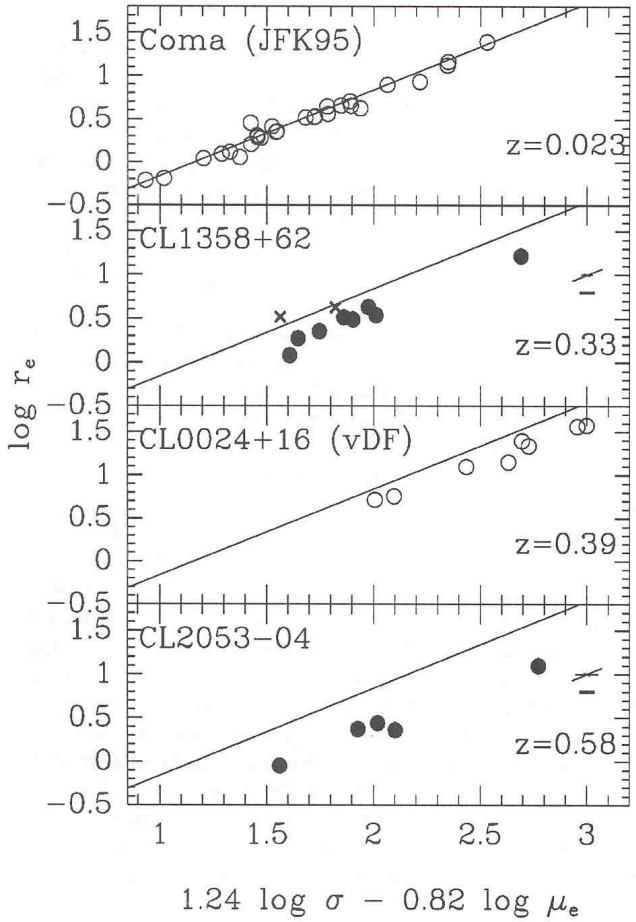

FIG. 2.—Fundamental plane for the four clusters, with the mean fundamental plane for Coma (JFK96) plotted on each panel. Note that the two E+A's in Cl 1358+62 (*crosses*) lie to the left of the mean relation of the "old" Cl 1358+62 early-type galaxies. The previous results of JFK96 and vDF are shown as open circles. The new data are shown as filled circles. Typical random errors (*thin bars*) and systematic errors (*thick bars*) are shown.

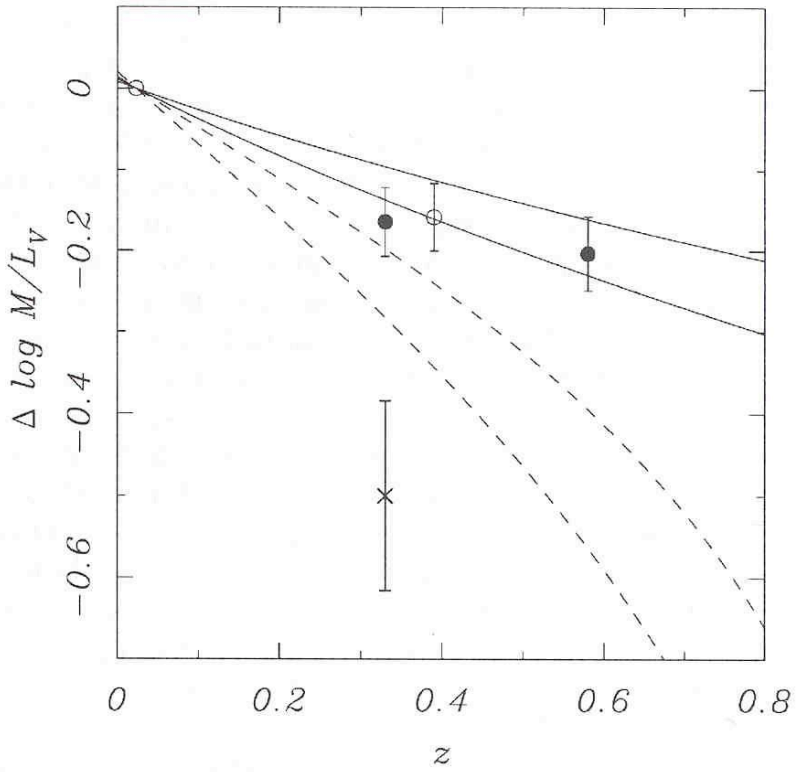

FIG. 3.—Mean M/L_V offsets with redshift, for $q_0 = 0.05$. The area enclosed by solid lines corresponds to single-burst models with $z_{form} = \infty$ and a range of initial mass functions. The region marked by dashed lines corresponds to the equivalent $z_{form} = 1$ models. The previous results of JFK96 and vDF are shown as open circles. The new data are shown as filled circles. The cross marks the M/L_V offset derived from the two E+A galaxies in Cl 1358+62. The errors were estimated by adding the random and systematic errors in quadrature.

(Kelson et al. 1997)

Elliptical Galaxies

General Properties Previously Highlighted

- Elliptical Galaxies have elliptical shapes with no structure
- Old stellar populations
- Very little gas & dust

But Some Have

- Counter-rotating cores
- $M(H_2) \sim 10^{7\text{-}9}\ M_{sun}$

These are probably Transition Galaxies

Counter-rotating Cores in Elliptical Galaxies

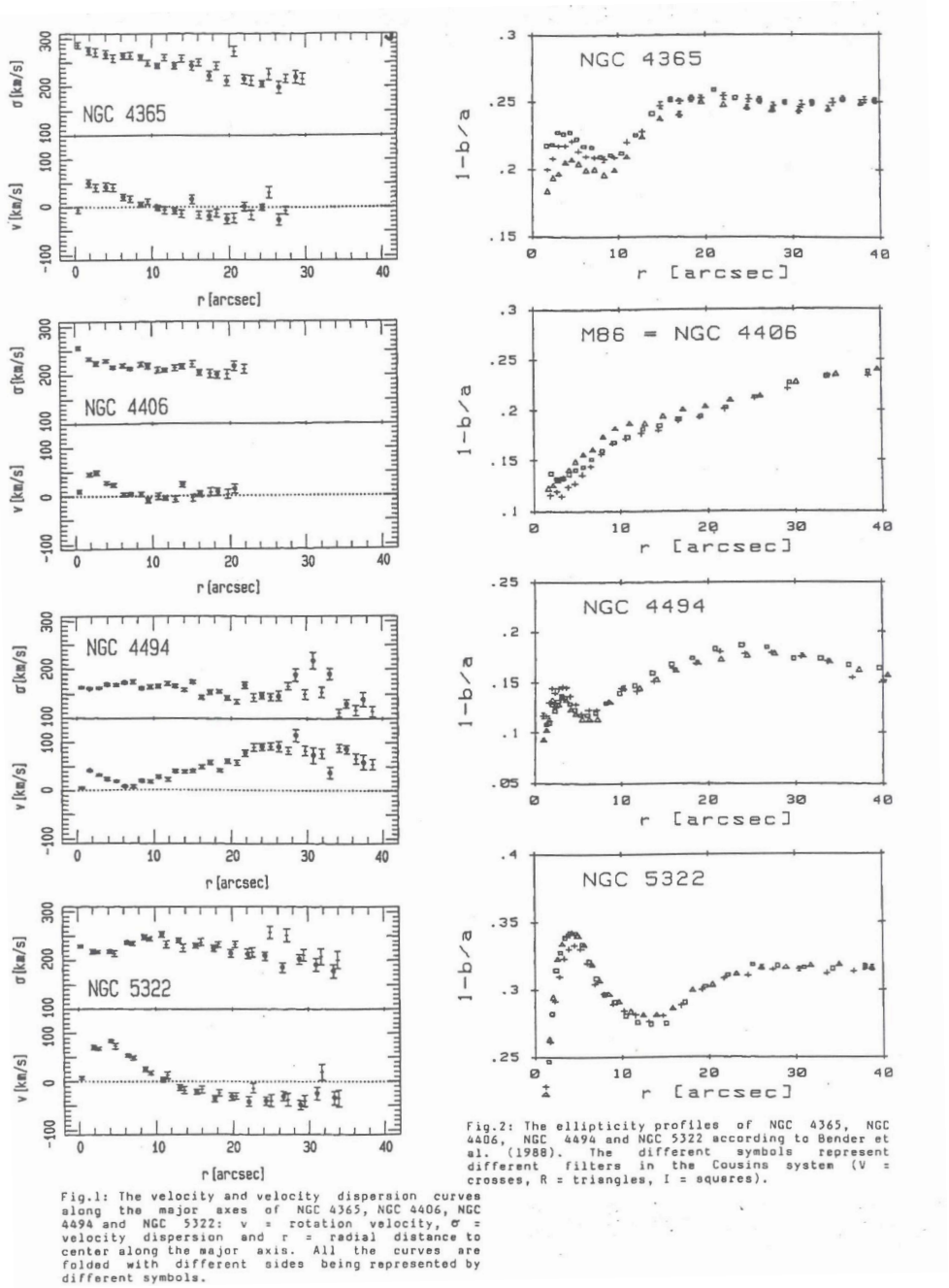

Fig.1: The velocity and velocity dispersion curves along the major axes of NGC 4365, NGC 4406, NGC 4494 and NGC 5322: v = rotation velocity, σ = velocity dispersion and r = radial distance to center along the major axis. All the curves are folded with different sides being represented by different symbols.

Fig.2: The ellipticity profiles of NGC 4365, NGC 4406, NGC 4494 and NGC 5322 according to Bender et al. (1988). The different symbols represent different filters in the Cousins system (V = crosses, R = triangles, I = squares).

(Bender 1988)

Molecular gas in Elliptical Galaxies

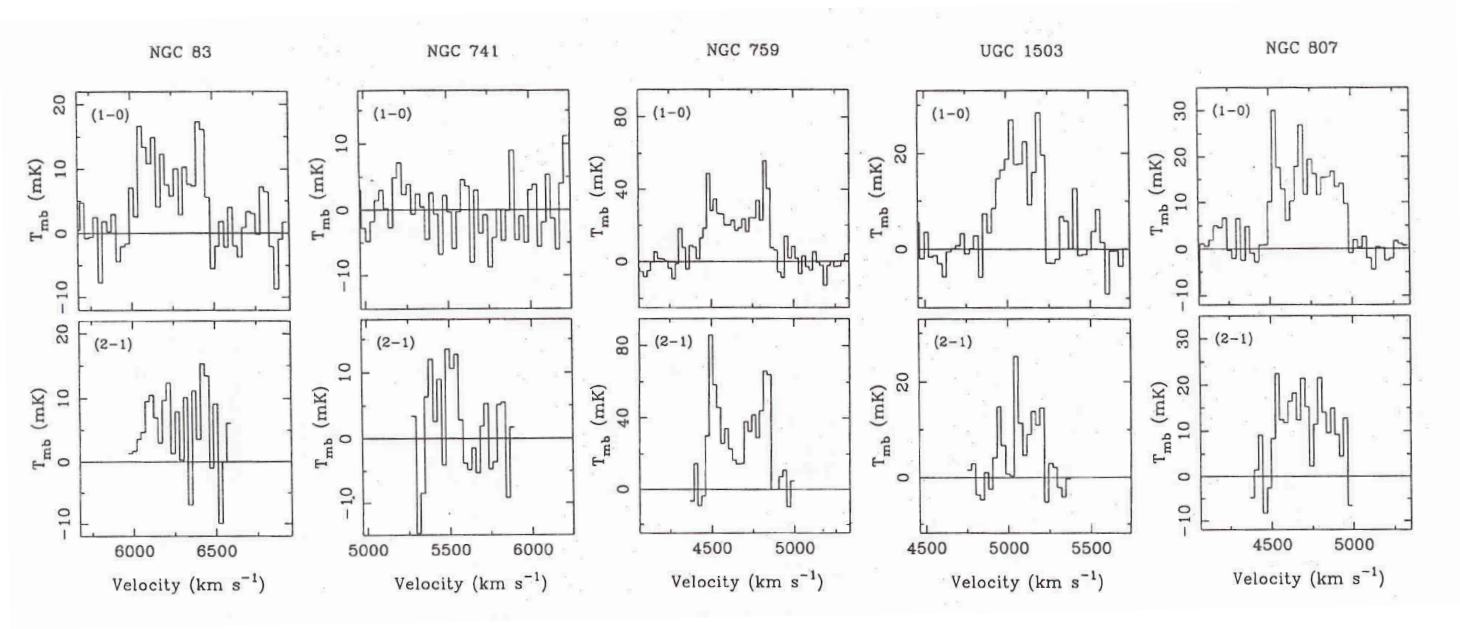

- $M(H_2) \sim 10^{7\text{-}9}\ M_{sun}$
- But these are IRAS-detected Elliptical Galaxies

(Lees et al. 1991; Wiklind & Combes 1995)

CO maps of Elliptical Galaxies

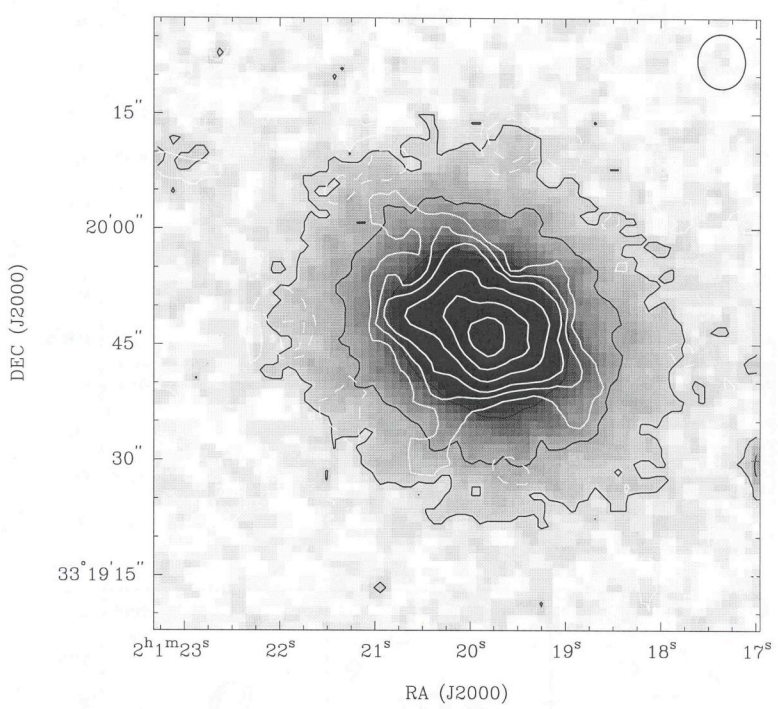

Fig. 3.— Molecular gas in UGC 1503. The greyscale and thin black contours are an optical image from the red portion of the second generation Digitized Sky Survey. The heavy white contours show the CO integrated intensity in units of −20, −10, 10, 20, 30, 50, 70, and 90 percent of the peak, which is 6.3 Jy b^{-1} km s^{-1} = 3.9×10^{21} cm^{-2} using the H_2/CO conversion factor described in Section 4.2. The small ellipse at the top indicates the size of the beam.

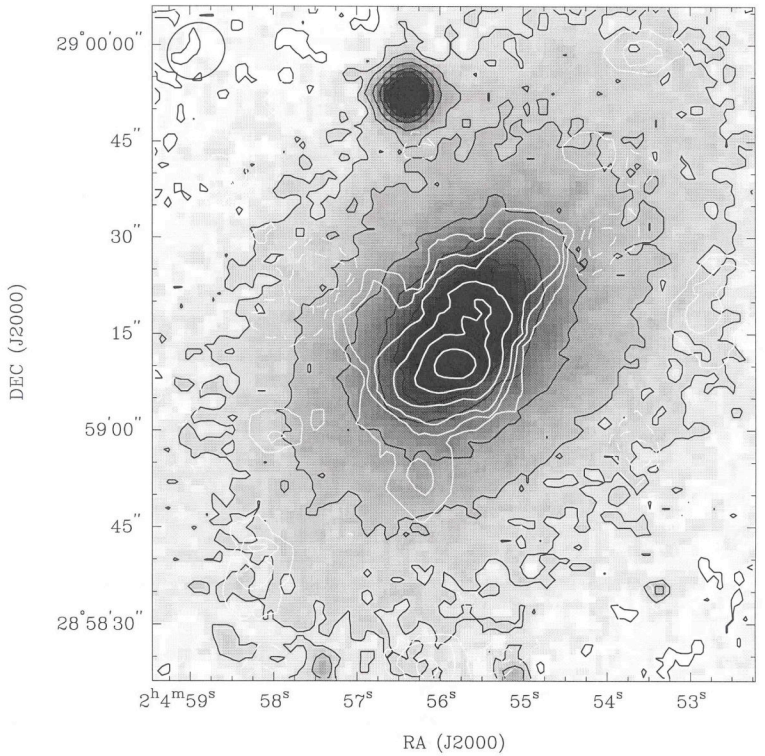

Fig. 8.— Molecular gas in NGC 807. Heavy white contours show the CO integrated intensity in units of −20, −10, 10, 20, 30, 50, 70, and 90 percent of the peak (7.6 Jy b^{-1} km s^{-1} = 2.6×10^{21} cm^{-2}). Other features as in Figure 3.

(Young 2002)

Gas Properties Relative to Infrared Emission

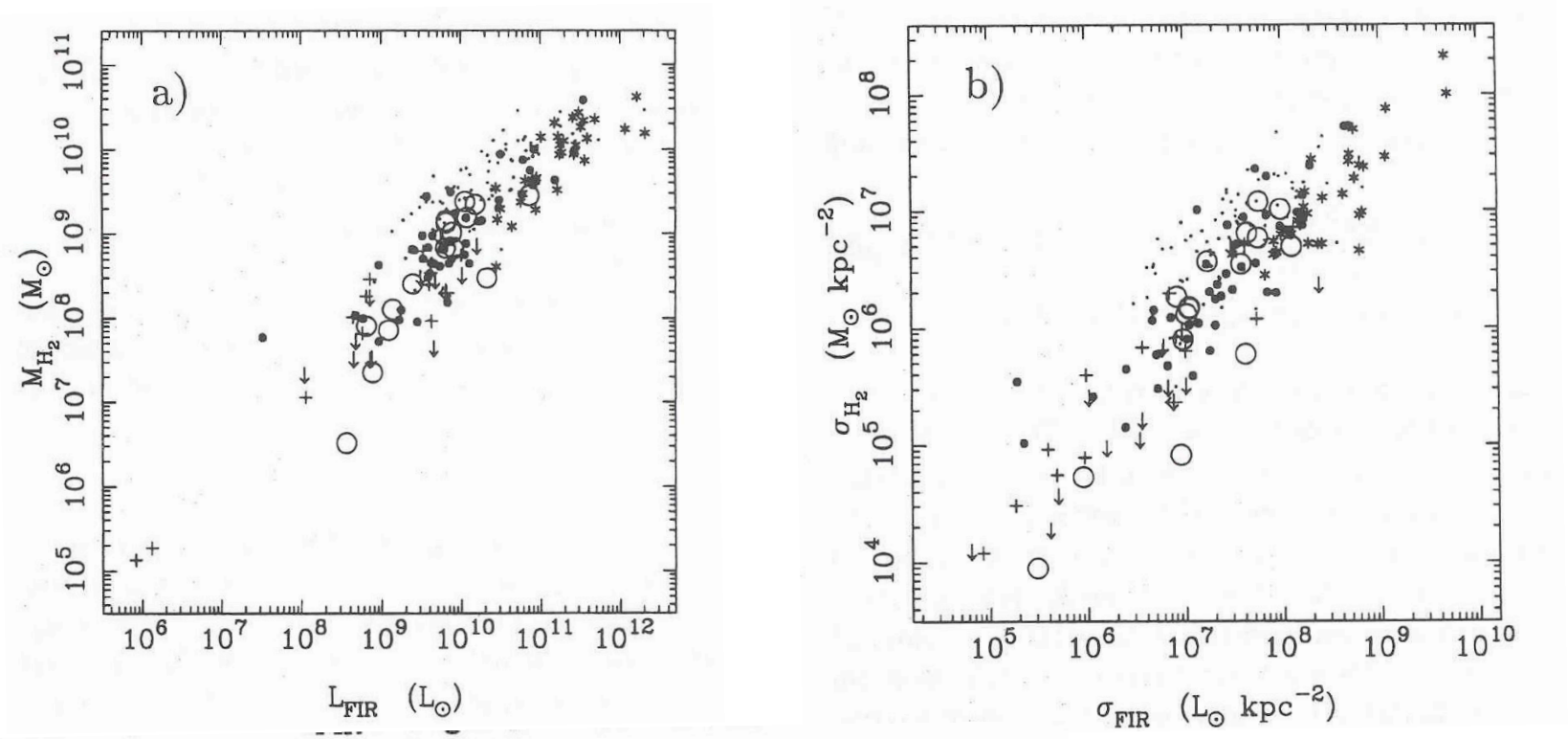

Fig. 3. a The molecular mass as a function of the FIR luminosity. Elliptical galaxies from our sample are plotted as open circles. For comparison we also plot some elliptical galaxies observed by others (crosses), lenticular galaxies (filled circles), normal spiral galaxies (dots) and ultraluminous FIR galaxies (stars). Upper limits are shown for our elliptical sample only and are represented by arrows. **b** The surface brightness of H_2 versus the surface brightness of the FIR luminosity

(Wiklind & Combes 1995)

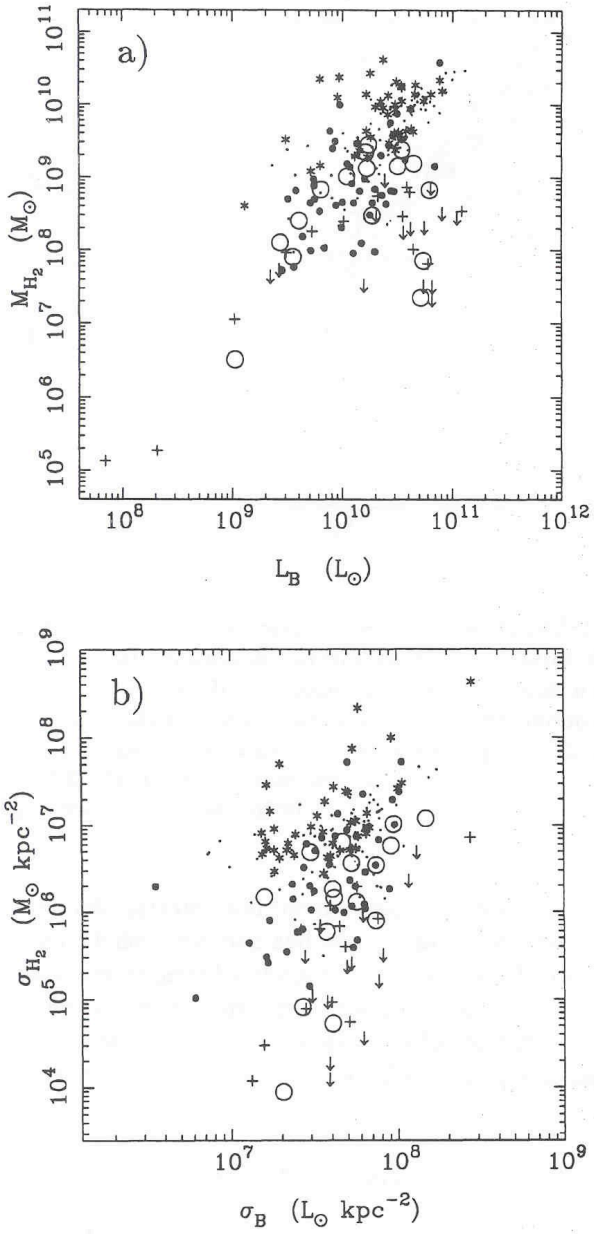

Fig. 4. a The molecular mass as a function of the blue luminosity. **b** The surface brightness of H_2 versus the surface brightness of the blue luminosity. Designations are the same as in Fig. 3

Relative to L_B

- Correlation with L_B is very poor.

(Wiklind & Combes 1995)